Quaternary Science Reviews 381 (2026) 109937

Contents lists available at ScienceDirect

Quaternary Science Reviews

journal homepage: www.elsevier.com/locate/quascirev

Quantifying quaternary climate variability in the Southern Caucasus using land snail shell isotope transfer functions and climatic niche modeling

Christiane Richter [a,*], Michael Schneider [a], Daniel Wolf [a], Frank Walther [b], Bernhard Hausdorf [c], Hayk Hovakimyan [d], Lilit Sahakyan [d], Markus Fuchs [e], Dominik Faust [a]

[a] Department of Geography, Dresden University of Technology, Germany
[b] Centre of Natural History, University Hamburg, Germany
[c] Leibniz Institute for the Analysis of Biodiversity Change, Hamburg, Germany
[d] Department of Geology, National Academy of Sciences of Armenia, Armenia
[e] Department of Geography, Justus-Liebig-University Gießen, Germany

ARTICLE INFO

Keywords:
Quaternary
Gastropods
Loess
Paleosol
Ecostratigraphy
Molluscs
$\delta^{18}O$
$\delta^{13}C$

ABSTRACT

Late Quaternary loess-paleosol sequences in the Armenian highlands represent key terrestrial archives for reconstructing past climate variability. Related proxy data are essential both for understanding the environmental and cultural history of the Caucasus area - a global biodiversity hotspot and archaeological key region - and for benchmarking Earth system models. However, robust quantitative paleoclimate records remain scarce for this climatically and topographically complex area. Here, we present a combined approach integrating (1) stable isotope analysis ($\delta^{18}O$, $\delta^{13}C$) of land snail shells with transfer functions build on modern calibration datasets and (2) probabilistic climatic niche modeling. For the latter, assemblage-weighted climatic optima are derived from species-specific response curves based on modern species distribution data. Our results reveal predominantly xerophilous faunas associated with colder glacial phases, and mesophilous high-grass to forest-steppe assemblages during interstadial and interglacial intervals. $\delta^{18}O_{shell}$ was used to reconstruct $\delta^{18}O_{precipitation}$ signals, which in this study area strongly correlate with temperature. Growing season temperature estimates, based on modern empirical relationships, suggest a mean difference of ~4.9 °C between glacial minima and interglacial maxima, while precipitation reconstructions from climatic niche modeling suggest a shift from ~511 mm to ~770 mm. This study provides the first mollusk-based quantitative reconstructions of Late Quaternary temperature and precipitation in the Caucasus area, demonstrating the potential of integrated mollusk proxies as powerful tools for resolving glacial-interglacial climate dynamics.

1. Introduction

Paleoclimatic and paleobiological data are crucial for understanding ecosystem responses to climatic change and identifying ecological tipping points. They also provide indispensable benchmarks for testing and refining process-based Earth System Models. However, many regions still lack robust quantitative paleoclimate records. The Caucasus represents both a global biodiversity hotspot (Myers et al., 2000) and a key corridor for human migrations since prehistoric times (Mellars, 2004; Gasparyan and Glauberman, 2022). Yet, quantitative constraints on its past climate remain fragmentary, as most existing studies provide only semi-quantitative or qualitative information. In the Armenian Highlands, well-preserved loess paleosol sequences span multiple glacial-interglacial cycles and form one of the most complete terrestrial archives in the region (Wolf et al., 2016, 2022; Lomax et al., 2021). Across Eurasia, loess-paleosol sequences have been widely recognized as sensitive recorders of Quaternary climate variability (Chu and Nett, 2021; Újvári et al., 2021; Sun et al., 2021; Lehmkuhl et al., 2023; Rousseau et al., 2023; Jia et al., 2024). In the Armenian Highlands, Richter et al. (2020) revealed clear glacial-interglacial faunal shifts in gastropod assemblages, but corresponding quantitative climate estimates were lacking. To fill this gap, we combine two complementary quantitative proxy approaches. First, we apply Mutual Climatic Range (MCR) analysis, refined through probabilistic niche modeling. The classical MCR approach (Atkinson et al., 1987; Bray et al., 2006), previously applied to Quaternary land snail faunas (Moine et al., 2002;

* Corresponding author.
E-mail address: christiane_richter@tu-dresden.de (C. Richter).

https://doi.org/10.1016/j.quascirev.2026.109937
Received 9 October 2025; Received in revised form 5 January 2026; Accepted 9 March 2026
Available online 19 March 2026

Grimley et al., 2020), is here enhanced by probabilistic species-climate response curves derived from modern species occurrence data, providing more realistic and constrained climatic optima. While such quantitative approaches have been developed in the 90's (Rousseau, 1991), they achieved recent advances by modern techniques such as increasing availability of high-resolution raster datasets for modern climate parameters and modeling tools used to quantify snail-climate responses (Dong et al., 2022; Wei et al., 2025). Second, we employ isotope-based transfer functions derived from the stable isotopic composition of land snail shells. The oxygen isotopic composition ($\delta^{18}O$) primarily reflects that of local precipitation ($\delta^{18}O_{precipitation}$) (Lécolle, 1985; Nield et al., 2022), although evaporative enrichment must be considered (Dettman et al., 2024). The $\delta^{18}O$ precipitation signal itself is controlled by temperature of the rain-bearing air masses, vapor source, precipitation amount and altitude among others (e.g., Dansgaard, 1964; Rozanski et al., 1993; Field, 2010), and has been widely used to infer past climate and atmospheric circulation patterns (Banak et al., 2016; Richter et al., 2021; Schmitt et al., 2024; Wang et al., 2024). In parallel, stable carbon isotope ratios ($\delta^{13}C_{shell}$) provide complementary information on the snail's diet, reflecting past vegetation composition and water availability (Metref et al., 2003; Liu et al., 2007; Yanes et al., 2008; Schmitt et al., 2025). By applying these combined approaches to loess-paleosol sequences in the Sevkar region (NE Armenia), we establish the first mollusk-based quantitative reconstruction of Late Quaternary temperature and precipitation in the Caucasus area. Beyond providing new insights into regional climate dynamics, this study highlights the potential of multi-proxy mollusk methods as a bridge between empirical paleoenvironmental records and Earth system model simulations in complex montane regions.

2. Study area

2.1. Geographical setting

The study area is situated in the north-eastern foothills of the Lesser Caucasus, within the Armenian Highlands (Fig. 1). As part of the Caucasus region, this area is particularly suitable for climate effect analyses due to its unique natural history that created a high level of endemism and highly sensitive ecosystems. The investigated loess section 'Achajur' (895 m a.s.l., 41°00′16″ N, 45°09′22″ E) belongs to the Sevkar loess area

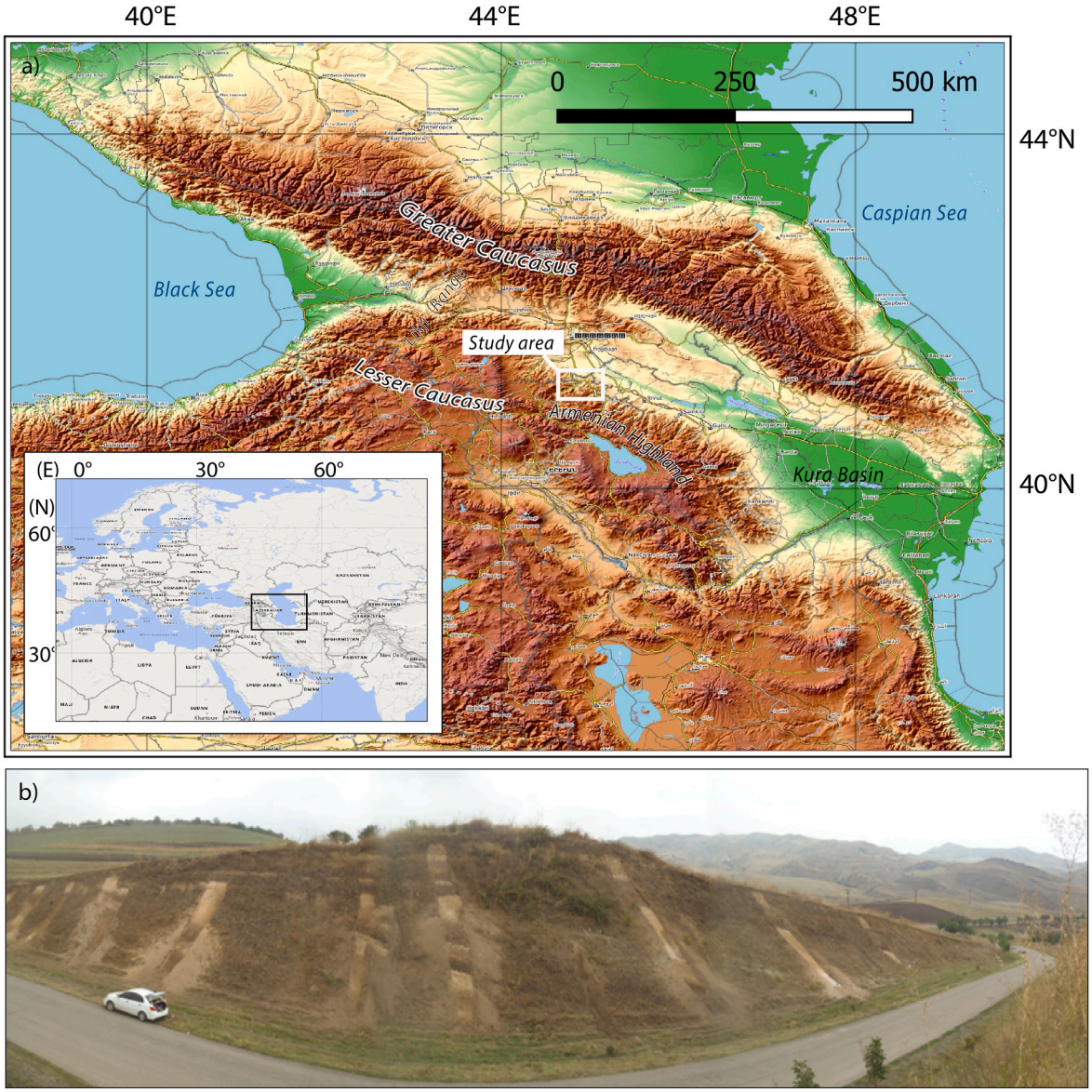

Fig. 1. Overview of the study area: a) Map showing the location of the Sevkar loess region within the Armenian Highlands, where the investigated sections Achajur and BL are located, b) Field photograph of loess profile prospection in the Sevkar region, showing distinct loess paleosol sequences near the town of Sevkar.

and is located near the Armenian village of Achajur in the Tavush province. Along with the section 'BL' (Borderline) (680 m a.s.l., 41°01′32.9″ N, 45°10′00.7″ E), it lies within the catchment of the Aghstev river, which ultimately drains into the Kura Basin, which is part of the larger tectonic depression between the Greater and Lesser Caucasus Mountains. Since the Pleistocene, the Greater Caucasus has acted as a climatic barrier, separating the southern parts, including the Lesser Caucasus foothills, from cold northern winds. As a result, parts of the Kura depression served as protected refugia during colder glacial phases (Zazanashvili et al., 2004). The Likhi Range further shields the study area from (humid) air masses coming from the Black Sea (Lydolph, 1977), leading to higher aridity in the Kura basin today. The present climate at the studied sites is characterized by average annual precipitation amounts of 481 mm at Achajur, with a mean annual temperature of 11.1 °C and mean growing season temperature (for all months ≥ 5 °C) of 15.5 °C, based on WorldClim v2 gridded data (Fick and Hijmans, 2017). At BL, precipitation amounts to 447 mm, mean annual temperature to 11.8 °C and growing season temperature to 15.1 °C.

2.2. Litho- and biostratigraphic background

The Quaternary terrestrial sediment sequences investigated in this study consist predominantly of loess, partially admixed with tephric material. These loess deposits are intercalated with pedocomplexes of multiple paleosols that formed during warmer climatic phases related to interglacial and interstadial periods (Wolf et al., 2022). The two loess sections BL and Achajur form the basis of the present gastropod-based proxy analysis. Detailed descriptions of the lithological units and chronology are provided by Wolf et al. (2022) and Lomax et al. (2021), respectively. An overview of the stratigraphic succession and age model is provided in Fig. 2. The lithostratigraphy at both sites did not reveal a clearly developed MIS 2 loess unit (discussed in detail in Wolf et al., 2022). Accordingly, the coldest interval of the last glacial might not be fully included in our dataset. First studies on fossil gastropod assemblages in loess-paleosol sequences of the Armenian Highlands were conducted by Richter et al. (2020), who developed an ecostratigraphic framework for the Quaternary deposits of the Sevkar region based on species compositions. Their results indicate consistent compositional shifts in the gastropod assemblages between loess and paleosol units. Loess units, predominantly corresponding to glacials (Lomax et al., 2021), were dominated by taxa characteristic of shrub- and shortgrass-steppe environments. These assemblages reflect semi-arid to arid climatic conditions but do not contain species characteristic of explicitly cold biomes. By contrast, the gastropod assemblages preserved

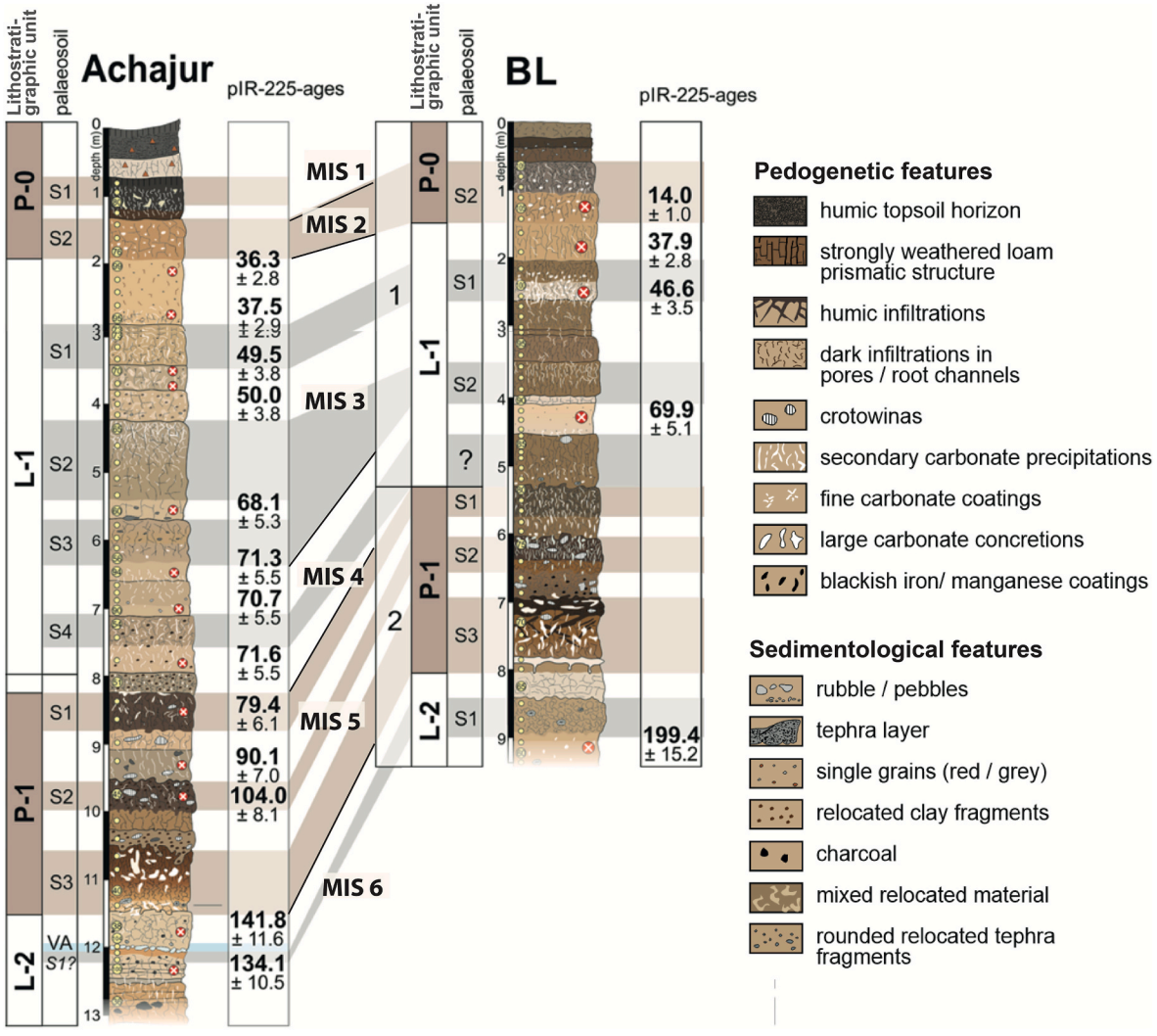

Fig. 2. Stratigraphic correlation of the loess sections Achajur and BL in the Armenian Highlands for the last two glacial-interglacial cycles, modified from Wolf et al. (2022). Paleosols within pedocomplexes P-0 and P-1 are indicated by brown coloring, representing phases of enhanced soil formation during generally warmer periods, while paleosols linked to glacial interstadials within loess units are highlighted with grey background. The correlation is supported by post IR-IRSL-225 chronology, see Wolf et al. (2022). (For interpretation of the references to color in this figure legend, the reader is referred to the Web version of this article.)

within pedocomplexes included species indicative of highgrass-to forest-steppe ecosystems, suggesting comparatively higher mean annual precipitation. Building on this litho- and biostratigraphic framework, the present study adds a new fossil record as well as modern gastropod calibration data and applies recently developed quantitative approaches to reconstruct Late Quaternary climate evolution in the Armenian Highlands.

3. Methods

3.1. Sediment sampling for subfossil gastropod analysis

To establish a robust dataset for the gastropod-based proxy analysis, we selected sections Achajur and BL as the most representative and complete sequences in the Sevkar loess region for our analyses. In the Achajur section, we collected 38 sediment samples over 13 m in accordance with lithological units of varying thickness. Exact sample positions are shown in Fig. 4. Each sample comprised 10 L of sediment. To extract gastropod shells, all samples were wet sieved to the fraction bigger than 500 μm. Given the high clay contents repeatedly exceeding 60%, causing strong grain aggregation, the sediment was agitated for 3 to 10 h before sieving. Extracted shells were identified using a stereomicroscope with 20 to 40 times magnification. Complete shells and shell fragments were separated and quantified following Ložek (1990). To complement the Achajur dataset, we also included samples from the BL section, for which mollusk assemblage data and related semi-quantitative interpretation have been previously published (Richter et al., 2020). For section BL, 30 samples were collected across 9 m using a similar sampling procedure. This study expands on the species assemblage data from both sections by integrating stable isotope and assemblage-weighted climatic range analyses for more refined quantitative paleoclimate reconstruction.

3.2. From mutual climatic range to probabilistic niche estimates

3.2.1. Modern species and climate data compilation

Climatic preferences of the studied species were determined based on their modern distributions within the wider Caucasus region and corresponding climate data (see Fig. 3). Modern distribution data were compiled from 1457 sites using both recent field collections and revised museum records elaborated within the scope of the "Biogeography of the Land Molluscs of the Caucasus Region" project (Hausdorf et al., data under preparation). For each species occurrence site, 19 bioclimatic parameters were extracted from the WorldClim database (Fick and Hijmans, 2017). From these, growing season temperatures were calculated as averages of all months with mean temperatures $\geq$5 °C. This 5 °C temperature threshold is applied here as an operational approximation of the activity phase of land snail species (see Lipińska et al., 2025), supported by the correlation of shell isotope signals with local precipitation isotopy, found i.a., by Richter et al. (2025). As measures for aridity, we used the Global Aridity Index from Zomer et al. (2022), defined as the ratio of mean annual precipitation to mean annual potential evapotranspiration. All climate data represent mean values for the period 1970 to 2000 at a spatial resolution of 30 arc seconds (~925 m grid cells). Although this resolution does not capture microclimatic heterogeneity in complex mountain terrain, it follows established practice, facilitating comparability and a robust first approximation at the regional level.

3.2.2. Climatic niche modeling using MaxEnt and ENMeval

To refine the climatic interpretation of the studied (sub)fossil assemblages, we use species-climate response curves, which represent the likelihood of a species occurring across a given climatic gradient. Unlike the classical MCR approach, which uses only minimum-maximum tolerances, such species-climate response curves provide full climatic preference profiles and optima. As a preparatory step, all candidate climate variables (see 3.2.1) were evaluated for their predictive power and interdependence with respect to modern species distributions in the Caucasus region. Univariate models were generated for each variable-species combination in the R package ENMeval (Muscarella et al., 2014) coupled to Maximum Entropy (MaxEnt) modeling (Phillips et al., 2006), using a constant 3-fold cross-validation across all predictors to ensure comparability. Model and predictor performance was assessed using three complementary metrics: (i) the corrected Akaike Information Criterion (AICc), which balances model fit against complexity (with lower values indicating better support, and a delta AICc of <2 between variables not significant); (ii) the area under the receiver operating characteristic curve (AUC), where 0.5 indicates random predictions and values close to 1.0 indicating high discriminative power; and (iii) the 10% omission rate, representing the proportion of presences incorrectly classified as absences when applying the 10th percentile training threshold (lower values indicating higher predictive ability). To avoid redundancy, variables were screened for multicollinearity, with pairwise Pearson correlation coefficients $R^2 > 0.7$ ($p < 0.005$) considered collinear (Dormann et al., 2013). From each resulting cluster, the variable combining the strongest predictive signal with the greatest paleoclimatic interpretability was retained. For the final predictor, species-specific response curves were generated with MaxEnt software v3.4.4 (Phillips et al., 2017), using a beta multiplier of 1.5, linear, quadratic and hinge features, the raw output format and 10.000 randomly selected background points. From these response curves, weighted means were then used to estimate the most probable climatic mean for their occurrence. For each (sub)fossil assemblage, sample-level climatic means were calculated by weighting the climate responses of individual species according to their relative abundance within an assemblage. Uncertainty ranges were expressed as the full mutual climatic range (MCR) defined by the overlap of all species-specific tolerance ranges within an assemblage, thereby yielding the broadest set of jointly tolerated climatic conditions.

3.2.3. Probabilistic climate reconstruction using CREST

In parallel to MaxEnt modeling, we applied CREST developed by Chevalier et al., 2014, 2022) originally designed for pollen-based climate reconstructions. CREST is a deterministic approach that derives probability density functions (PDFs) for each taxon and combines them to generate assemblage-level reconstructions. In this study, we implemented CREST with newly compiled land snail calibration data, since gastropods were not yet included in the standard CREST database. Calibration in the CREST R package was performed using weighted cumulation of species PDFs to account for relative abundances. Our own distributional data were incorporated via the function `crest.set_modern_data`. From the resulting cumulative, abundance-weighted posterior PDFs of the fossil assemblages, we report both mean climatic optima and the 5 - 95% probability interval as the uncertainty range.

3.3. Stable isotope analysis of (sub)fossil shells and modern reference data

To reconstruct paleoclimatic conditions from loess-paleosol sequences, we also analyzed the stable oxygen and carbon isotopic composition ($\delta^{18}O$ and $\delta^{13}C$) of subfossil gastropod shells from the BL and Achajur sections. All isotope analyses were performed on shells of *Kalitinaia crenimargo*, a species consistently present throughout both sections and thus suitable for systematic comparisons across the sections. In total, 14 samples from the BL section and 20 samples from the Achajur section were analyzed, using 3 to 4 shells per sample. Before analysis, all shells were cleaned in an ultrasonic bath and treated with 10% hydrogen peroxide (H_2O_2 by volume) to remove residual organic matter. The samples were then rinsed with tap water, air-dried, and powdered using an agate mortar and pestle. Stable isotope measurements were carried out at the Department of Human Evolution, Max Planck Institute for Evolutionary Anthropology in Leipzig, using a

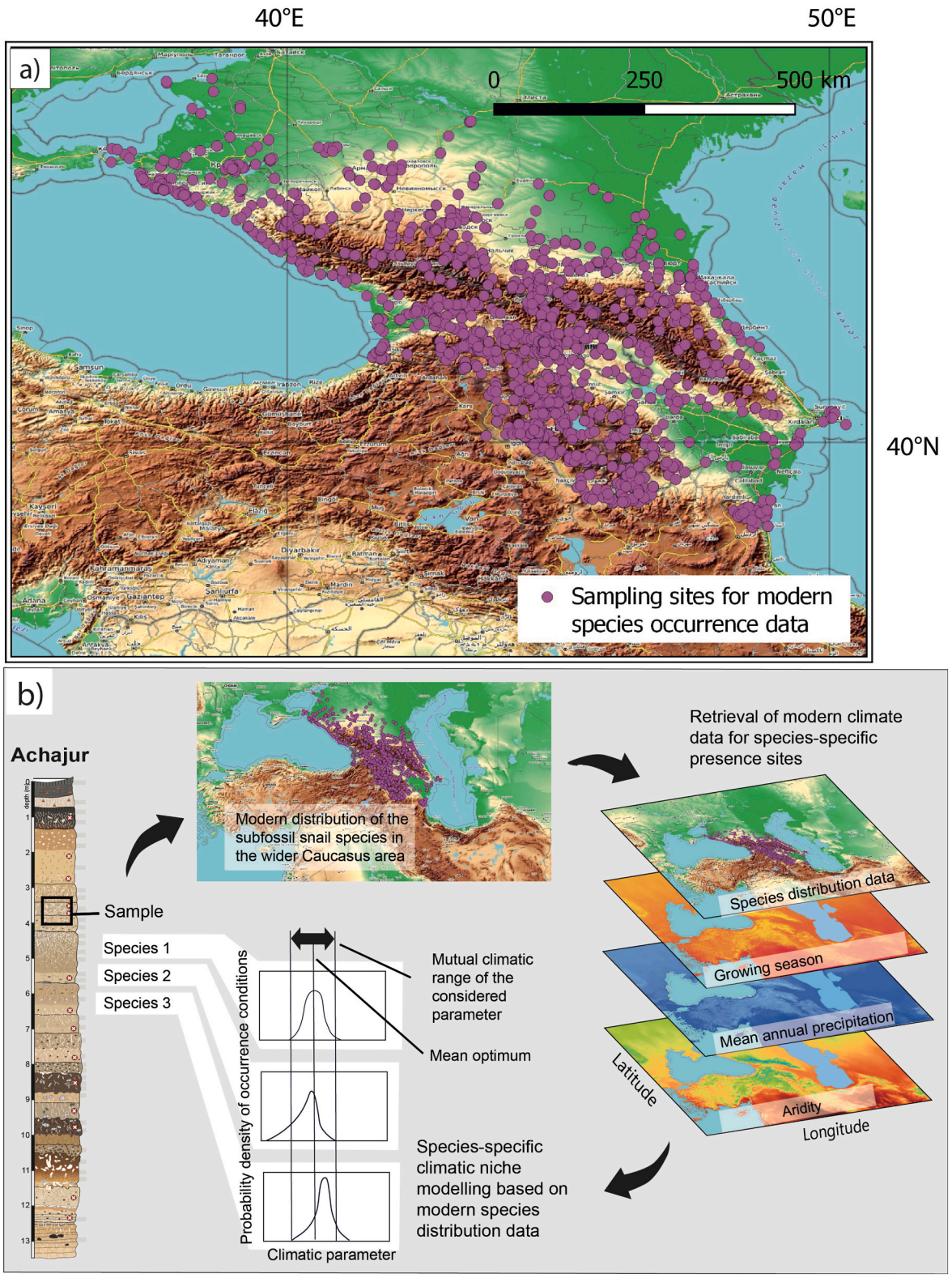

Fig. 3. (a) Modern sampling sites of the relevant snail species in the wider study area. (b) Schematic overview of the methodical approach: Species-specific climatic niches are modeled based on modern distribution data to identify probability-weighted climatic optima of each species. Using occurrence- and abundance-based weighting of these species-specific climatic optima in each assemblage, we calculated mean climatic values for each sample (abundance-weighted mean optima). The values obtained form the basis for quantitative precipitation reconstructions across the loess sections Achajur and BL.

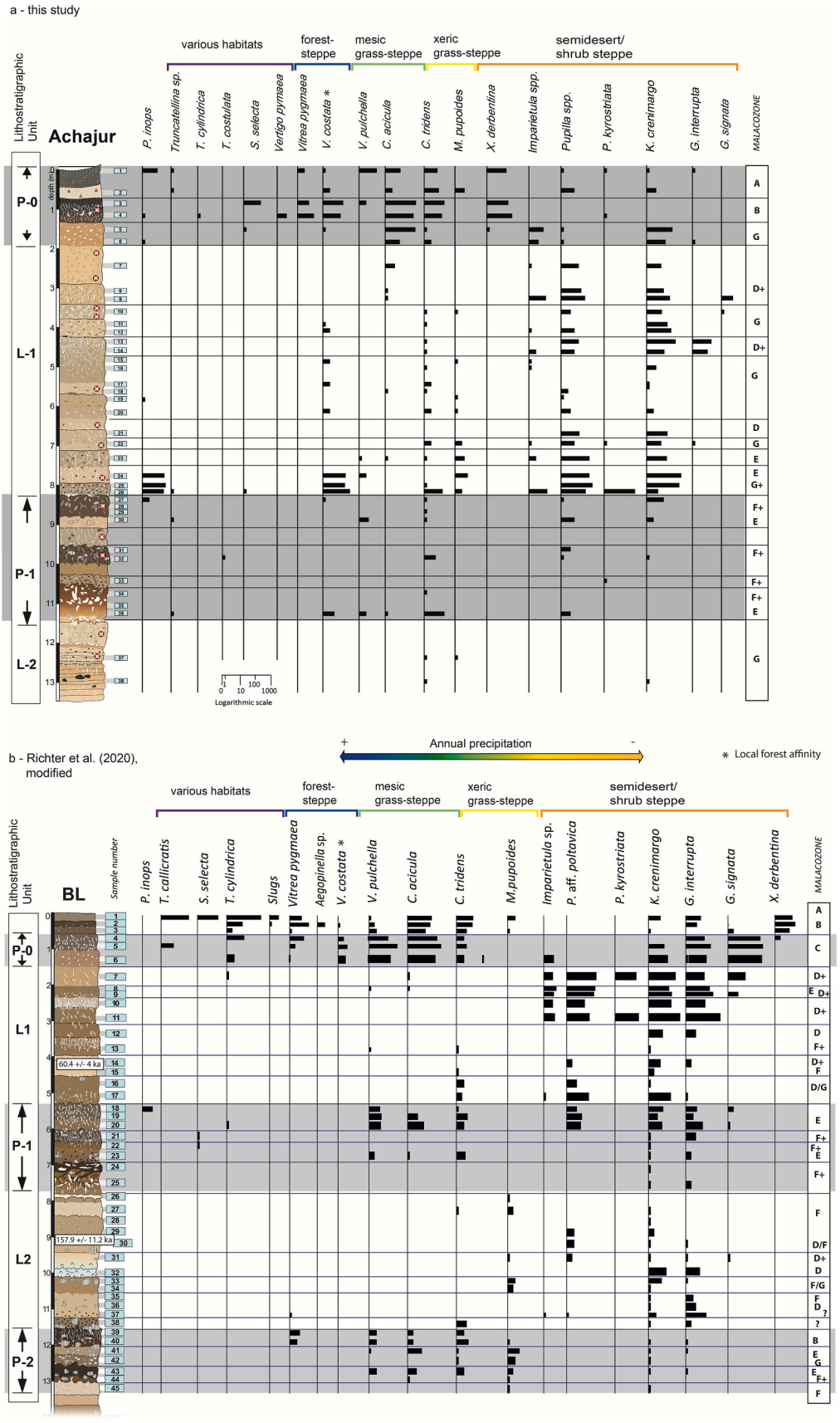

(caption on next page)

Fig. 4. Distribution of gastropod taxa across the Achajur section, including their ecological classification and assignment to malacozones following Richter et al. (2020). For comparison, we depicted the mollusk assemblages from the upper part of the BL section published in Richter et al. (2020), which this study expands upon in part of its analysis. A more detailed description of malacozones can is provided in Fig. 7 and Richter et al. (2020). The numbered rectangles indicate the sampling positions. Furthermore, the weighted mean precipitation optima for each assemblage are shown on the right. Note that the full mutual ranges (range bars) remain broadly constant along the profile because even single rare occurrences extend the cumulative tolerance window, whereas the weighted mean is sensitive to relative abundances and therefore better captures stratigraphic trends.

Thermo Fisher 253 Plus gas source isotope ratio mass spectrometer coupled to a Kiel IV automated carbonate preparation device. Isotope values are reported in delta (δ) notation in per mill (‰) relative to the Vienna Pee-Dee Belemnite (VPDB) standard. Calibration was performed using the international reference material IAEA-603 (Carrara marble; $\delta^{18}O = -1.64‰$, $\delta^{13}C = +1.87‰$). Analytical precision (1σ) was better than ±0.1‰ for both $\delta^{18}O$ and $\delta^{13}C$.

To support the climatic interpretation of the subfossil shell isotope data, we analyzed a modern reference dataset from the Sevkar loess region. For the closest present relative, *Stenomphalia selecta*, 10 shells per site were collected and measured for stable isotope composition at four locations, including the Achajur and BL sections. Site information and raw data are provided in supplementary Table_S1 (sheet 'Modern shell d18O Sevkar area').

3.4. Transfer functions for $\delta^{18}O_{precipitation}$ and temperature estimation

To reconstruct past precipitation isotopes ($\delta^{18}O_{precipitation}$), we used $\delta^{18}O$ values from (sub)fossil snail shells ($\delta^{18}O_{shell}$) as proxies, applying an empirical transfer function. This function is based on the modern calibration datasets published by Lécolle (1985) and Zanchetta et al. (2005), which demonstrate a strong correlation between $\delta^{18}O_{shell}$ and $\delta^{18}O_{precipitation}$ across Europe. For our recalibration, we performed linear regression using updated high-resolution modern precipitation isotope datasets from the RCWIP2 model (Terzer-Wassmuth et al., 2021), provided by the International Atomic Energy Agency (IAEA). RCWIP2 offers improved spatial precision (30 arc seconds) with a reported root mean square error (RMSE) of 1.29‰, thereby refining the original interpolated $\delta^{18}O_{precipitation}$ data. The precipitation isotope values extracted from this dataset (monthly means, annual averages and growing season means for months >5 °C) are provided in the supplementary Table_S1 (sheet 'Modern shell d18O literature'). To derive near-surface air temperatures from the reconstructed $\delta^{18}O_{precipitation}$ values, we applied the modern empirical relationship found for the Armenian highlands by Brittingham et al. (2019). Their data indicate a shift of 0.49‰ in $\delta^{18}O_{precipitation}$ per each 1 °C shift in temperature, relating to following regression equation: $\delta^{18}O = -14.31 + 0.49\ T°C$ ($r^2 = 0.55$, $p < 0.001$; SE = 4.1‰). This relationship was applied to $\delta^{18}O_{precipitation}$ values reconstructed from $\delta^{18}O_{shell}$ data of our study.

Uncertainty estimates for $\delta^{18}O_{precipitation}$ reconstructions were calculated using Gaussian error propagation, combining the standard error of the applied transfer function with the standard errors of the used shell means (derived from within-assemblage standard deviations and sample size). For temperature reconstructions based on precipitation isotopes, uncertainties were further propagated through the precipitation-temperature regression. For range estimates, the uncertainty was increased to account for differencing two independent endpoints, by combining their uncertainties in quadrature.

4. Results

4.1. Subfossil gastropod record Achajur

The gastropod fauna of the investigated Achajur section comprises at least 20 terrestrial species of the following taxa: *Aegopinella* indet., *Cecilioides acicula* (Müller, 1774), *Chondrula tridens* (Müller, 1774), *Gibbulinopsis interrupta* (Reinhardt in Martens, 1876), *Gibbulinopsis signata* (Mousson, 1873), *Imparietula* indet. , *Kalitinaia crenimargo* (Pfeiffer, 1848), *Multidentula pupoides* (Krynicki, 1833), *Pupilla bipapulata* Akramowski, 1943, *Pupilla kyrostriata* Walther and Hausdorf, 2014, *Pupilla inops* (Reinhardt, 1877), *Pupilla* aff. *poltavica* Boettger, 1889, *Pupilla triplicata* (Studer, 1820), *Stenomphalia selecta* (Klika, 1894), *Truncatellina callicratis* (Scacchi, 1833), *Truncatellina cylindrica* (Férussac, 1807), *Vallonia costata* (Müller, 1774), *Vallonia pulchella* (Müller, 1774), *Vitrea pygmaea* (Boettger, 1880), *Xeropicta derbentina* (Krynicki, 1836). Species compositions and abundances for each sample are depicted in Fig. 4. The subdivision of the section into malacozones follows the classification by Richter et al. (2020), based on both presence and abundance data of the species. An overview of the defined malacozones is provided in Fig. 7. The older pedocomplex P-1 between 11.5 and 8.2 m depth (samples AJ-36 to AJ-27) exhibits just low shell preservation, likely due to intensified decalcification related to pedogenesis (see calcium carbonate contents in Wolf et al., 2022). Despite the scarcity of shells, the preserved specimens are taxonomically diverse and characteristic of malacozone E, including *Vallonia pulchella*, *Vallonia costata*, *Chondrula tridens* and *Truncatellina*. The upper, Holocene pedocomplex P-0 (2 to 0 m depth) shows a high diversity in mesophilous taxa, including *Vitrea pygmaea* and *Aegopinella*. This assemblage reflects high-grass to forest steppe environments and corresponds to malacozones A, B, and G. In contrast, the loess layers outside the pedocomplexes (between 13.4 to 11.5 m and 8.2 to 2 m depth) yielded xerophilous assemblages assigned to malacozones D, D+ and G. These are dominated by taxa such as *Kalitinaia crenimargo*, *Gibbulinopsis interrupta*, *Gibbulinopsis signata* and *Pupilla kyrostriata*, typically associated with shrub and shortgrass-steppe ecosystems. A detailed dataset of species occurrences and abundances is provided in supplementary Table_S2 (sheets 'Moll_Table AJ' and 'Moll_Table BL').

4.2. From mutual climatic range to probabilistic niche estimates

4.2.1. Climatic niche modeling using MaxEnt and ENMeval

The new dataset of modern gastropod distributions from the wider Caucasus region, used for climatic niche modeling, comprises 1457 georeferenced records described in detail in supplementary Table_S3. These records formed the basis for evaluating climatic predictors. Multicollinearity screening revealed strong correlations among the 20 candidate variables across all occurrence sites, summarized in the correlation matrix and clustering dendrogram (Fig. 5). In further predictor testing, precipitation of the warmest quarter yielded the lowest AICc values for 12 of 15 species and achieved the highest mean AUC (0.88) with relatively low 10% omission rates (~0.11), underlining its strong statistical signal. However, this variable captures only a narrow seasonal window and is therefore problematic for paleoclimatic applications, as glacial-interglacial shifts likely altered precipitation seasonality in ways that cannot be reliably reconstructed. Within the collinear precipitation cluster, annual precipitation produced slightly less optimal fits (mean AUC = 0.85; omission ~0.13) but still clearly outperformed temperature related predictors such as mean annual temperature (AUC = 0.65), mean temperature of the warmest quarter (AUC = 0.78), or minimum temperature of the coldest month (0.54), all of which showed substantially weaker discriminatory power. Because annual precipitation integrates overall water availability and is less sensitive to temporal changes in seasonality, it represents the most suitable and ecologically robust predictor for paleoclimatic reconstructions, balancing statistical performance with interpretability. Accordingly, we used mean annual precipitation for subsequent analyses. Fig. 6 shows the species-climate

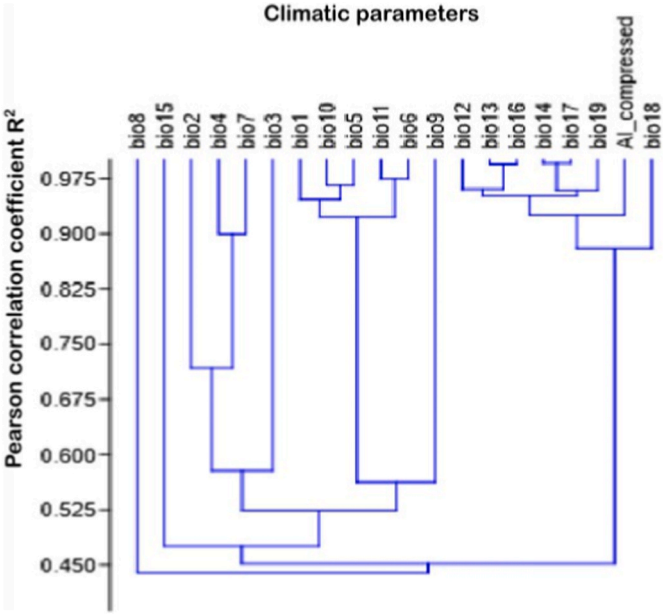

Fig. 5. Dendrogram showing the correlation among climatic predictors taken from BioClim (Fick and Hijmans, 2017) and Zomer et al. (2022). Temperature-related variables: bio1 – Annual Mean Temperature (°C), bio2 – Mean Diurnal Range (°C) = mean of monthly (Tmax − Tmin), bio3 – Isothermality (%) = (bio2/bio7) × 100, bio4 – Temperature Seasonality (standard deviation of monthly temperature × 100), bio5 – Max Temperature of Warmest Month (°C), bio6 – Min Temperature of Coldest Month (°C), bio7 – Temperature Annual Range (°C) = bio5 − bio6, bio8 – Mean Temperature of Wettest Quarter (°C), bio9 – Mean Temperature of Driest Quarter (°C), bio10 – Mean Temperature of Warmest Quarter (°C), bio11 – Mean Temperature of Coldest Quarter (°C). Precipitation-related variables: bio12 – Annual Precipitation (mm), bio13 – Precipitation of Wettest Month (mm), bio14 – Precipitation of Driest Month (mm), bio15 – Precipitation Seasonality (Coefficient of Variation), bio16 – Precipitation of Wettest Quarter (mm), bio17 – Precipitation of Driest Quarter (mm), bio18 – Precipitation of Warmest Quarter (mm), bio19 – Precipitation of Coldest Quarter (mm). Additionally, the AI_compressed variable represents the aridity index (Zomer et al., 2022). Predictors exceeding a pairwise Pearson correlation coefficient of $R^2 > 0.7$ ($p < 0.005$) are considered collinear and clustered accordingly.

response curves for mean annual precipitation derived from modern species distributions, with weighted mean optima for each taxon provided in supplementary Table_S4 (sheet 'MaxEnt species niches'). Assemblage-level most probable precipitation means, and associated mutual climatic ranges are shown alongside the stratigraphic section (Fig. 4), while the full dataset and related calculations are provided in supplementary Table_S4 (sheet 'MaxEnt + CREST results AJ & BL').

For the BL section, the lowest value of the most probable mean annual precipitation estimate was obtained for loess unit L2 (sample BL-31), with a weighted mean of 515 mm a mutual climatic range for all species in this assemblage (MCR) of 363 - 600 mm, characteristic of a strongly xerophilous community. At the other end of the spectrum, the subrecent colluvial layer of pedocomplex P0 (sample BL-1) yields the highest most probable mean annual precipitation estimate with a weighted mean of 770 mm (MCR 447 - 738 mm), followed by pedocomplex P2 (sample BL-39) with a weighted mean of 723 mm (MCR 447 - 792 mm). Mesophilous assemblages are consistently associated with higher reconstructed precipitation means (median 640 mm), while xerophilous assemblages relate to substantially lower values (median 539 mm; Mann-Whitney *U* test: $r = 0.68$; $p < 0.001$).

A similar pattern emerges in the Achajur section. Here, the lowest value was observed in loess unit L1 (AJ-9), with a weighted mean of 511 mm (MCR 363 - 600 mm), whereas the highest precipitation estimates stem from the subrecent colluvium of pedocomplex P0 (AJ-1) with 720 mm (MCR 449-738 mm) and pedocomplex P-1 (sample AJ-30 and AJ-36) with 717 and 715 mm. Again, mesophilous assemblages (median 640 mm) are significantly wetter than xerophilous ones (median 539 mm; Mann-Whitney *U* test, $p < 0.001$).

4.2.2. Probabilistic climate reconstruction using CREST

To facilitate direct comparison of our precipitation estimates with other studies employing PDF-based climate reconstructions with biological proxies, we additionally applied the more widely used CREST framework (Chevalier et al., 2014), which moreover yields an explicit uncertainty range derived from the cumulative probability density (see Methods chapter). Both approaches capture the same overall gradient between xerophilous and mesophilous communities, and loess units and pedocomplexes, respectively, with minor systematic differences in absolute values (Table_S4). For the AJ section, the lowest most probable precipitation mean reconstructed with MaxEnt for loess unit 1 of 511 mm (AJ-9) closely matches the CREST estimate of 465 (−154/+238) mm. The highest mean values with MaxEnt of 719 mm in P-0 and 716 mm in P1 are also in good agreement with CREST results yielding 722 (−306/+557) mm in P0 and 664 (−266/+480) mm in P1. The median values of xerophilous assemblages yield 532 mm in MaxEnt compared to 495 mm in CREST, while mesophilous communities reach 635 mm in MaxEnt but only 525 mm in CREST. Also pedocomplex medians plot wetter in MaxEnt (675 mm) than in CREST (578 mm). The BL section follows the same trend. Here, the driest assemblage shows lowest values in loess unit L2 with 515 mm in MaxEnt and 467 (−161/+244) mm using CREST. The wettest assemblages amount to 770 mm in P0 and 723 mm in P1 when using MaxEnt and to 683 (−388/+906) mm and 765 (−191/+252) mm, respectively, when using CREST. Yet, as in AJ, medians values of xerophilous versus mesophilous communities differ more strongly, yielding 552 mm in MaxEnt and 506 mm using CREST for xerophilous assemoblages, while mesophilous ones show a median of 638 mm in MaxEnt and 538 mm using CREST. Pedocomplex medians average 638 mm in MaxEnt and 537 mm in CREST. In summary, CREST tends to return systematically lower median precipitation values than MaxEnt, while both approaches reproduce the overall climatic gradients in a consistent manner.

4.3. Stable isotope results

4.3.1. Carbon

Carbon stable isotope data measured from the subfossil shells of *K. crenimargo* are presented in Fig. 7, with the full datasets available in supplementary Table_S1 (sheet 'Paleo shell δ13C'). The medians of the $\delta^{13}C_{shell}$ signals span a range of 2.4‰ across the BL section (−4.1‰ to −6.5‰, SD 1.2‰ and 1.8‰, respectively) and of 1.5% in the Achajur section (−5.8‰ to −7.2‰, SD 0.2‰ and 1.0‰, respectively). Despite these differences in overall variability, statistical testing (Wilcoxon rank tests and Kruskal-Wallis tests for multiple groups) consistently showed no significant relationship between $\delta^{13}C_{shell}$ values and either lithological units (pedocomplexes vs. loess layers) or ecological groups (xerophilous vs. mesophilous assemblages) in both sections. Medians of $\delta^{13}C_{shell}$ values were effectively identical between xerophilous and mesophilous assemblages (−5.5‰ vs. −5.5‰ at BL; −6.3‰ vs. −6.3‰ at AJ), as well as between pedocomplexes and loess layers (−5.7‰ vs. −5.5‰ at BL; −6.4‰ vs −6.3‰ at AJ). Accordingly, $\delta^{13}C_{shell}$ values do not exhibit systematic stratigraphic trends or consistent associations with ecological groupings or paleoenvironmental phases.

4.3.2. Oxygen

Oxygen isotope data (Fig. 7, Table_S1) from subfossil gastropod shells show systematic variations in $\delta^{18}O_{shell}$ values across the stratigraphic sequences. In the Achajur section, $\delta^{18}O_{shell}$ median values range from −1.1‰ in sample AJ-24 (within pedocomplex P-1, malacozone E) to −3.2‰ in sample AJ-14 (unit L1, malacozone D), reflecting a total range of 2.1‰ and a mean within-sample standard deviation of 0.6‰.

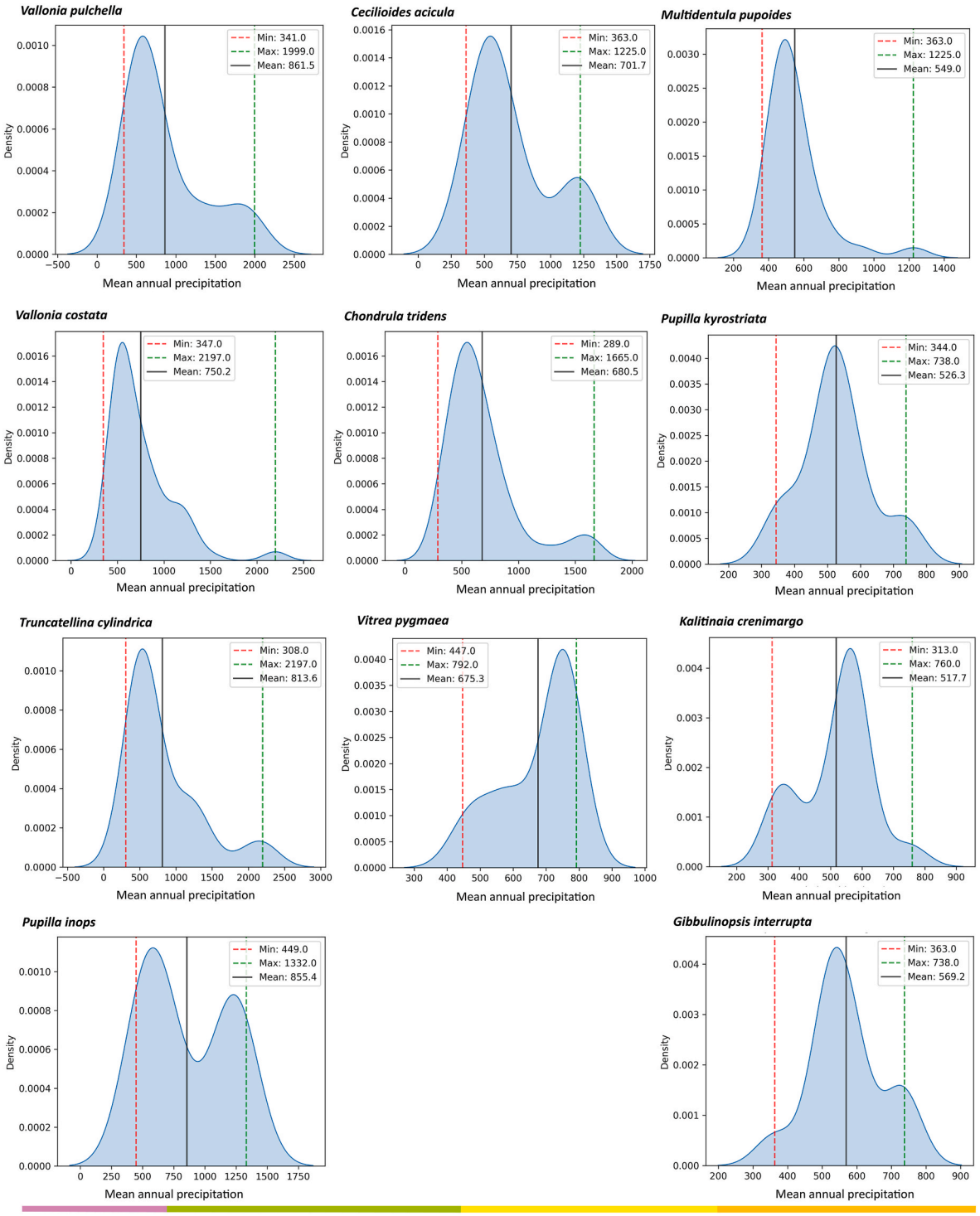

Fig. 6. Species-climate response curves for mean annual precipitation for each species, based on their modern distribution across the Caucasus region (see Sections 3.2 and 4.2 for methodical details). Dotted lines indicate the minimum (red) and maximum (green) precipitation values at which the species occur, as well as the mean precipitation optimum (black line). Unimodal curves suggest a stronger, more consistent association between species presence and precipitation values, whereas distinctly bimodal patterns may reflect additional environmental controls or broader ecological tolerances influencing the species' distribution. Response curves were interpreted only within the range of precipitation values observed in the training data; extrapolated values outside this range (e.g. < 0 mm) are not ecologically meaningful. (For interpretation of the references to color in this figure legend, the reader is referred to the Web version of this article.)

The BL section exhibits a broader range, with values extending from −0.5‰ in sample BL-19 (pedocomplex P-1, malacozone E) to −3.8‰ in BL-11 (loess unit L1, malacozone D), corresponding to a total range of 3.3‰ and a mean standard deviation of 0.5‰. A Kruskal-Wallis test indicates statistically significant differences in $\delta^{18}O_{shell}$ medians between stratigraphic units in both sections: $\chi^2 = 32.65$ (df = 12, p = 0.001) at BL and $\chi^2 = 31.06$ (df = 17, p = 0.02) at Achajur. Moreover, $\delta^{18}O_{shell}$ values vary systematically related to specific ecological assemblage types. Assemblages dominated by mesophilous species, corresponding to malacozones A, B, C, E and G (samples AJ-2, AJ-5, AJ-6, AJ-10, AJ-11, AJ-16, AJ-22 to AJ-27 and BL-5, BL-6, BL-17 to BL-20) exhibit more positive $\delta^{18}O_{shell}$ values. In contrast, assemblages

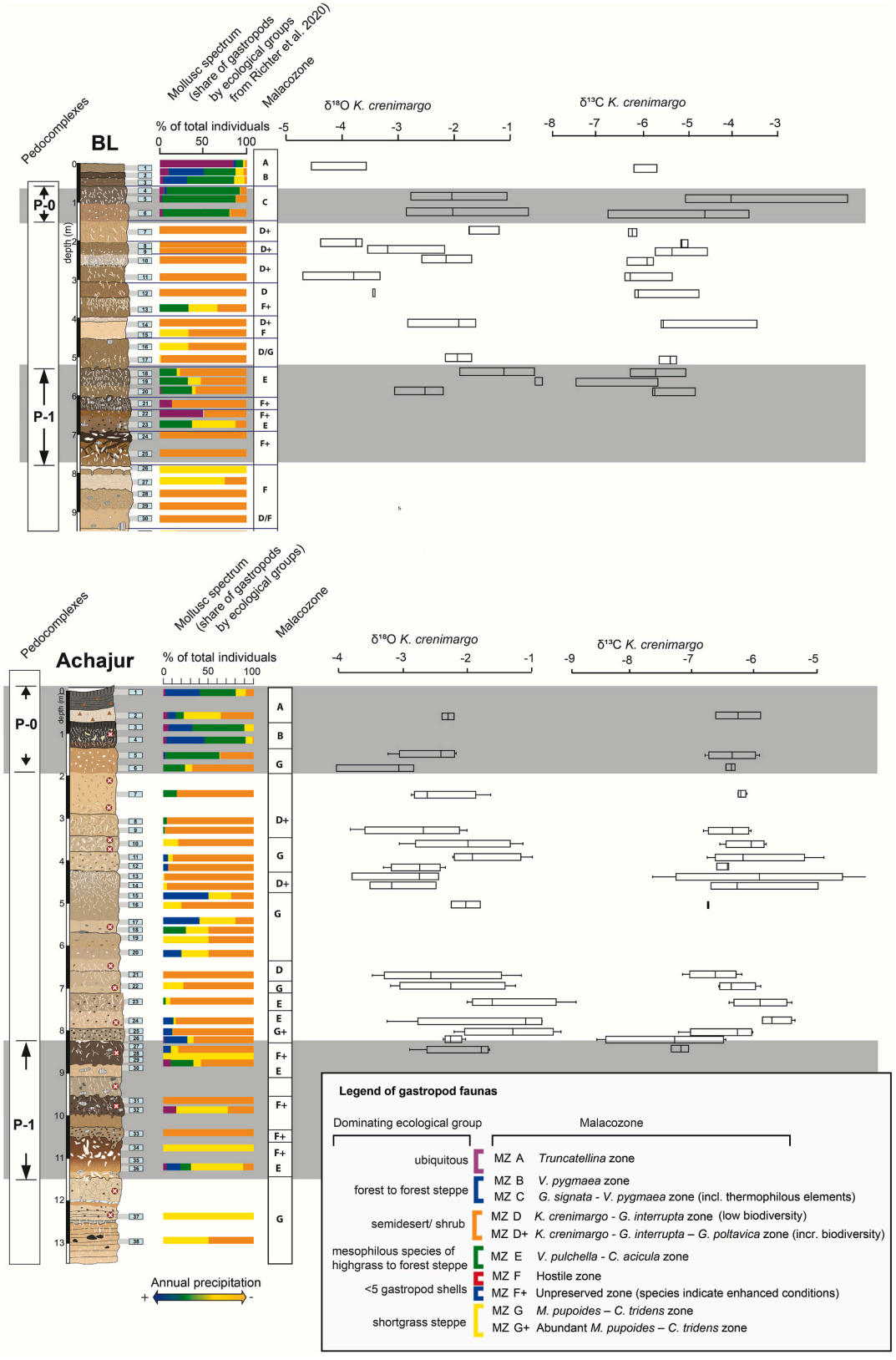

Fig. 7. Overview of mollusk assemblages displaying their species composition by ecological groups (color-coded bars), and stable isotope results. The relative abundance of gastropod taxa is presented as percentage bars for each sample. Stratigraphic columns on the left show lithological units and pedocomplexes (P-0, P-1) with corresponding malacozones (MZ A to G+) defined by dominant ecological groups (see box on the lower right). Boxplots on the upper right display $\delta^{18}O$ and $\delta^{13}C$ values measured from subfossil *K. crenimargo* shells for each sample. Note the correspondence of certain malacozones with shifts in $\delta^{18}O$ values, as well as differences between pedocomplexes and loess units. Ecological groups (legend lower right) range from ubiquitous to xerophilous taxa, supporting the environmental interpretation based on isotopes and species composition. (For interpretation of the references to color in this figure legend, the reader is referred to the Web version of this article.)

composed exclusively of xerophilous species, represented by malacozone D (samples AJ-7, AJ-9, AJ-12 to AJ-14, AJ-21 and BL-7 to BL-14) yield more negative values. A Mann-Whitney *U* test confirms that $\delta^{18}O_{shell}$ values differ significantly between assemblages dominated by mesophilous versus xerophilous species ($r = 0.58$, $p = 0.001$), with median values of −1.9‰ and −2.8‰, respectively (Fig. 8).

As comparison, modern shells of *Stenomphalia selecta* show median $\delta^{18}O_{shell}$ values of −1.56‰ at Achajur and −1.7‰ at BL (Table 1), placing them near the upper, most positive end of the paleo sample spectrum.

4.3.3. $\delta^{18}O_{shell}$ - derived $\delta^{18}O_{precipitation}$ values and related temperature estimates based on transfer functions

To reconstruct past $\delta^{18}O_{precipitation}$ values, we applied an empirical transfer function based on modern calibration datasets. In our regional dataset from the Sevkar loess area, $\delta^{18}O_{shell}$ values exhibit a strong correlation with modeled $\delta^{18}O_{precipitation}$ values ($r = 0.97$, $p = 0.032$). Given the limited size of this local dataset, we extended the calibration by incorporating published data from Lécolle (1985) and Zanchetta et al. (2005), including all available records for Helicoids, which belong to the same superfamily as *Kalitinaia crenimargo*. Across this expanded dataset, $\delta^{18}O_{shell}$ values remained strongly correlated with modeled $\delta^{18}O_{precipitation}$ values for growing season ($r = 0.65$, $p < 0.001$). The derived regression equation based on this expanded dataset is:

$$\delta^{18}O_{precipitation(GS)} = -6.4 + 0.73 \times \delta^{18}O_{shell} \quad (SE = 0.8, R^2 = 0.46) \qquad (1)$$

We apply this equation to the fossil shell data and get reconstructed $\delta^{18}O_{precipitation}$ values ranging from −6.8‰ (SE ± 0.8‰) to −9.3‰ (SE ± 0.9‰) in the BL section and from −7.3‰ (SE ± 0.9‰) to −8.8‰ (SE ± 0.9‰) in the Achajur section, with the largest reconstructed range of 2.4‰ (SE ± 1.2‰) observed in the BL section.

Related paleotemperature estimates based on the empirical relationship between $\delta^{18}O_{precipitation}$ and temperature from the Armenian Highlands published by Brittingham et al. (2019) suggest a mean growing season temperature difference of up to 4.9 °C between glacial minima and interglacial maxima at the BL section, with combined uncertainty using Gaussian method (see Methods chapter) of SE ± 6.8 °C. At Achajur, this maximum range amounts to 3.1 °C (SE ± 6.8 °C). Notably, interglacial and interstadial phases exhibit partly overlapping values, indicating relatively minor climatic differences between these intervals.

Median $\delta^{18}O_{shell}$ values from modern specimens amount to −1.6‰ (SD ± 0.8‰) at Achajur and −1.7‰ (SD ± 0.8‰) at BL, yielding shell-derived $\delta^{18}O_{precipitation}$ values of −7.6‰ (SE ± 1.1‰) and −7.7‰ (SE ± 1.1‰), respectively.

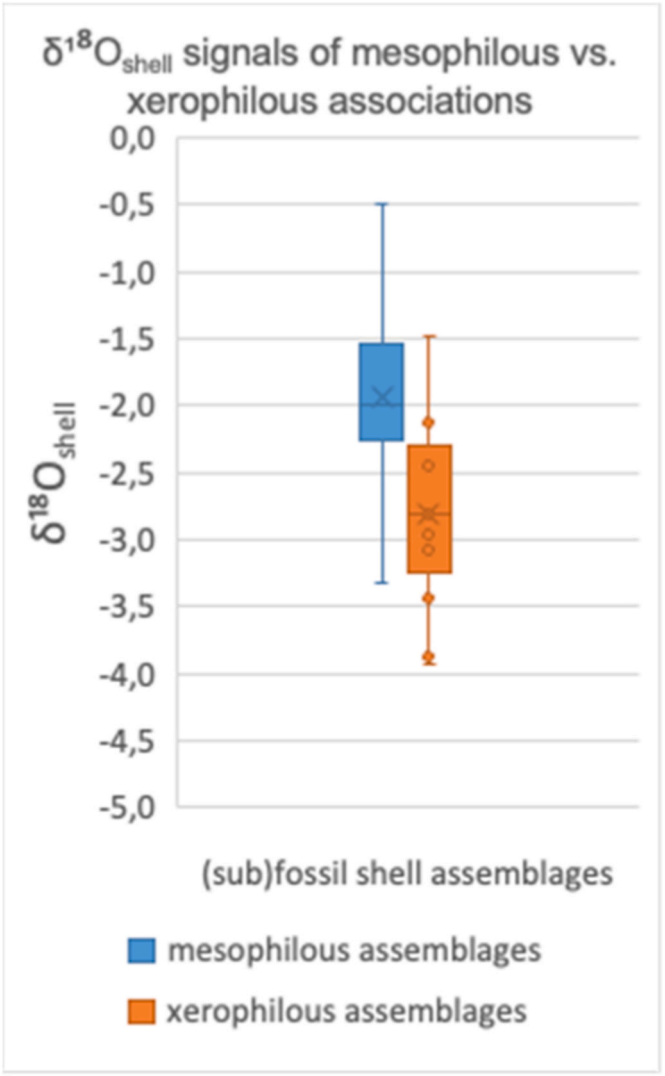

Fig. 8. Box-and-whisker plots of $\delta^{18}O_{shell}$ signals for mesophilous vs. xerophilous (sub)fossil land snail assemblages. Boxes indicate interquartile ranges; whiskers show the data range; the cross marks the mean while the dot denote an outlier. Group differences are evaluated in the text.

5. Discussion

5.1. Ecological transitions across glacial-interglacial cycles inferred from subfossil land snail assemblages

The diagnostic value of land snail assemblages for paleoenvironmental reconstruction has been demonstrated in numerous studies (e.g., Alexandrowicz et al., 2014; Horsák et al., 2019; Sümegi, 2019; Dong et al., 2022; Rousseau et al., 2023). In the Achajur section, they reveal a clear ecological turnover between loess and paleosol units, reflecting repeated environmental shifts between glacial and interglacial conditions. Loess units L2 and L1 at Achajur are associated with predominantly xerophilous taxa characteristic of dry shrub and shortgrass steppe, indicating arid glacial conditions. Their species composition closely matches that of the equivalent loess layers at BL (Fig. 4), implying regional steppe expansion during glacial phases. By contrast, the malacofauna of both pedocomplexes (P-1 and P-0) at Achajur shows an increase in mesophilous taxa. Although shell preservation is poor in P-1, the presence of *Vallonia pulchella* and *Vitrea pygmaea*, both indicative of increased moisture, points to higher humidity during interglacial conditions. Similar gastropod assemblages in the stratigraphically equivalent unit at BL (P-1, malacozone E) reinforce the regional coherence of this signal aligning with previous studies by Richter et al. (2020), linking these intervals to high-grass to forest steppe vegetation. The increased species richness in the upper pedocomplex P-0 suggests enhanced ecological complexity and vegetation heterogeneity within the Holocene, whereas *Stenomphalia selecta* and *Xeropicta derbentina* are typical elements of anthropogenically influenced or degraded environments. The high abundances of both species may indicate localized habitat disturbance caused by grazing or other forms of human land use.

An exception to these ecostratigraphic patterns occurs in samples AJ-24 to AJ-26, which contain unexpectedly high abundances of shells and a high number of mesophilous taxa, including *Pupilla inops* and *Vallonia costata*. As this layer (8.2 to 7.8 m depth) also contains a high amount of clay pebbles, we attribute it to a colluvial origin and link these high shell abundances to enrichment due to mixing with reworked soil sediments from the underlying pedocomplex. Paleoecological inferences from this unit should therefore be made with caution. Outside this interval, both the Achajur and BL records show a consistent alternation of xerophilous and mesophilous assemblages that track glacial-interglacial cycles. The

Table 1
Modern reference $\delta^{18}O_{shell}$ data for shells of *Stenomphalia selecta* collected in the Sevkar loess region. Values represent medians of each 10 measured shells per site.

Locality	Species	No. of shells	Median $\delta^{18}O_{shell}$ ‰ VPDB	$\delta^{18}O_{shell}$ Std.Dev.	$\delta^{18}O_{precipitation}$ (>5 °C)	$\delta^{18}O_{precipitation}$ Mean annual
Sevan Pass	*S.selecta*	*10*	−2.41	0.78	−9.79	−12.68
Sevkar	*S. selecta*	*10*	−1.40	0.88	−7.82	−8.60
Achajur	*S. selecta*	*10*	−1.56	0.80	−7.93	−8.96
BL	*S. selecta*	*10*	−1.70	0.83	−7.87	−8.66

malacological signal aligns with other long-term proxy data in the wider region, like pollen data from Lake Urmia (Djamali et al., 2008) and Lake Van (Litt et al., 2014; Pickarski and Litt, 2017). All these records indicate *Artemisia*-dominated shrub steppe during colder glacial phases and rising proportions of arboreal elements, such as *Quercus, Betula* and *Juniperus* during interglacials, supporting a coherent regional climate signal.

5.2. Quantitative assessment of climatic changes using species distribution modeling

While species compositions already indicated recurrent shifts between xerophilous and mesophilous communities, species-climate response curves allowed these qualitative trends to be translated into quantitative differences in precipitation. Median assemblage-weighted climatic optima in pedocomplexes varied from those of loess units by ~85 mm at Achajur and ~98 mm at BL, while loess units occasionally include moister interstadial phases. Minima in loess layers amount to ~510 mm annual precipitation, whereas pedocomplex and colluvial layers reached up to 770 mm. These amplitudes of up to 260 mm demonstrate that transitions from stadial loess to interglacial soil formation involved substantial shifts in effective water availability. However, reconstructed estimates for glacial intervals of over 500 mm do not coincide with a dominance by grassland and shrubland taxa. Such totals are unusually high for open vegetation and may partly reflect a systematic upward bias in our precipitation estimates. Likewise, estimates approaching ~770 mm per year imply comparatively humid conditions for forest-steppe associations. In modern Eurasia, forest-steppe typically occurs under annual precipitation means of ~420 to 650 mm (Chytrý et al., 2022; Erdős et al., 2019), with higher amounts often relating to thermal constraints or disturbance through land-use and pasturing (Erdős et al., 2019). However, the latter are unlikely for the pre-Paleolithic units in our sections. For a systematic overestimation, two sources of bias are particularly relevant. First, xerophilous taxa such as *Pupilla* aff. *poltavica* or *Imparietula* spp. could not be included in the assemblage-weighted calculations, due to unresolved taxonomy and missing distribution data. This reduces the weight of dry-adapted species. Second, modern baselines may already be altered by anthropogenic land-use, as shrub expansion in semi-arid areas is often driven by grazing and disturbance rather than natural aridity. Both effects tend to bias reconstructions towards wetter conditions, pushing estimates to the upper ecological limits of modern analogues. Despite these uncertainties, the reconstructions remain robust in their relative trends. The MaxEnt-based results converge with CREST outputs regarding climatic extremes, with driest loess-unit assemblages clustering around 515 mm (within the reconstructed uncertainty range) and pedocomplex units/soil sediments in colluvial layers surpassing 720 mm. This methodical agreement reinforces confidence in the reconstructed amplitudes, even if absolute values are inflated. In this sense, the models are reliable in capturing the magnitude and direction of hydroclimatic change rather than exact precipitation totals, confirming that glacial–interglacial transitions in the southern Caucasus were marked by ecologically significant differences in water availability. However, future work should further focus on modern calibration, comprehensively testing the niche modeling approach with respect to anthropogenic bias.

5.3. Quantitative assessment of climatic changes using shell isotope signals

5.3.1. Limitations of vegetation inference from $\delta^{13}C$ due to species-specific diet

Stable carbon isotope values ($\delta^{13}C$) from terrestrial gastropod shells are commonly used to infer dominant vegetation types, distinguishing e.g. between xerophilous C_4 and CAM plants and mesophilous C_3 vegetation (Yanes et al., 2013; Colonese, 2017). In our dataset, however, *median $\delta^{13}C_{shell}$ values of xerophilous and mesophilous grouped assemblages were effectively identical* across both sections (see Results chapter for detailed results). Likewise, no consistent offsets were observed between $\delta^{13}C_{shell}$ medians from loess units and pedocomplexes. These findings suggest that $\delta^{13}C_{shell}$ in this case does not reflect clear stratigraphic or community-level vegetation changes within the studied loess-paleosol sequences. While the small samples sizes may limit the ability to detect such differences, the observed patterns could also result from the complexity of assimilated carbon sources. In particular, the trophic ecology of *K. crenimargo* remains poorly understood with respect to its preference for C_3 vs. C_4/CAM plant material. Related taxa, such as *Xerolenta obvia,* have been reported to feed on both fresh and decaying plant matter (Schmid, 1930), while observations on *Cernuella virgata* and *Helicella itala* indicate a diet including decomposed vegetation and herbivore feces (Butler, 1972; Schmid, 1934; Frömming, 1954). This trophic flexibility may result in $\delta^{13}C$ values that reflect a mixture of organic carbon sources, thereby obscuring potential vegetation-specific signals. Although $\delta^{13}C$ analyses offer valuable insights into dietary behaviour, their applicability as a proxy for past vegetation composition and associated humidity conditions is limited in this study. A better understanding of taxon-specific feeding startegies is needed, as $\delta^{13}C$-based vegetation inferences are not straightforward in this context.

5.3.2. $\delta^{18}O_{shell}$ as quantitative proxy for past precipitation isotopy and climatic parameters

$\delta^{18}O$ values in gastropod shells constitute a widely used proxy for reconstructing past hydrological and climatic conditions. Since $\delta^{18}O_{shell}$ tracks $\delta^{18}O_{precipitation}$, we calculated paleo precipitation isotope values using taxon-specific regression functions (see Methods and Results). Although ^{18}O enrichment related to plant water uptake and perspiration, as well as the timing of shell growth or microhabitat conditions may influence shell isotope values (Goodfriend et al., 1989; Dettman et al., 2024), the systematically more negative $\delta^{18}O$_shell values observed in xerophilous assemblages argue against dominant evaporative enrichment and instead point to $\delta^{18}O$_prec as the primary controlling factor. In BL, the observed range between means of mesophilous and xerophilous assemblages differs by up to 3.3‰ in $\delta^{18}O_{shell}$ (with within-sample standard deviations in the respective samples BL11 and BL19 ≦ 0.7‰). This corresponds to a reconstructed precipitation-isotope shift of approximately 2.4‰ (±1.2‰, uncertainty reflecting Gaussian error propagation, see Methods chapter). While $\delta^{18}O_{precipitation}$ is on a global scale correlated with temperature, local variations can be strongly influenced by altitude, continentality, and source effects (see Rozanski et al., 1993). These, in turn, interact with broader factors such as global ice volume and atmospheric circulation patterns, which varied throughout the temporal range represented by the sequence. Whereas $\delta^{18}O_{precipitation}$ can be compared directly with other precipitation isotope records, the derivation of temperature requires application of

appropriate isotope-enabled atmospheric circulation models. Brittingham et al. (2019) did empirical studies on precipitation isotopy across the Armenian Highlands analysing samples from 475 precipitation events of eight localities. They found that, despite significant differences in source signals related to individual rain events, temperature explains most of the variance in $\delta^{18}O_{precipitation}$ in this area ($r = 0.74$, $p < 0.001$), whereas source-related effects are much weaker ($r = -0.35$, $p < 0.001$). They also found, that atmospheric circulation and related predominant moisture sources were strongly influenced by NAO variability. Negative NAO phases allowed greater input of isotopically heavier Mediterranean-sourced moisture from the south, compared to more negative signals from the Black Sea, which dominates under dominantly westerly influence. Extending this relationship to glacial-interglacial cycles at the Armenian highlands is difficult since atmospheric circulation patterns during glacial periods were likely fundamentally different from those of interglacial stages. Following Obreht et al. (2017), a stronger influence of the Siberian cold high-pressure system during glacial periods likely weakened the westerlies, potentially allowing isotopically heavier Mediterranean-sourced precipitation to reach Southern Caucasia. This could have further enriched the $\delta^{18}O$ signal of precipitation, which was elevated due to globally enriched $\delta^{18}O$ in marine source signals during glacial phases. However, this mechanism is not evident in our data: instead of enriched $\delta^{18}O$ values that would be expected for a shift towards Mediterranean sources under weakened westerlies, the glacial samples exhibit markedly more negative $\delta^{18}O$ values. This suggests that either the influence of southerly moisture sources was minor, or that the colder climate led to a stronger temperature-driven isotope depletion that overprinted any source-related enrichment. Alternatively, if Mediterranean input did increase, the observed values may actually underestimate the full extent of glacial cooling, as a potentially positive offset was masked or neutralized. We therefore assume that temperature remained the dominant control on shell $\delta^{18}O$, while acknowledging that glacial-interglacial circulation changes likely introduced additional but unquantified variance. Since we do not observe isotopic shifts of a magnitude consistent with major changes in moisture origin, we apply the $\delta^{18}O$-temperature transfer function as a first-order approximation. The resulting paleotemperature reconstructions should be interpreted within this framework, recognizing that the full glacial signal may be underestimate due to possible source effects acting in the opposite direction and further glacial-interglacial differences like seasonality or the intensity of evaporative effects on shell signals due to different aridity or wind strength. For the modern climate dynamics, Brittingham et al. (2019) report a shift of 0.47‰ in $\delta^{18}O_{precipitation}$ for each 1 °C shift in temperature. Applying our transfer function (Equation (1)) elaborated in Chapter 4.3.3., this makes a temperature shift of 1.5 °C for each 1‰ change in $\delta^{18}O_{shell}$ for our study area, coinciding with results from Lécolle (1985) for Europe, who calibrated a temperature shift of 1.4 to 2.3 °C for each 1‰ change in $\delta^{18}O_{shell}$. If we adopt the empirical relationship between $\delta^{18}O_{precipitation}$ and $\delta^{18}O_{shell}$ for the Armenian Highlands from Brittingham et al. (2019), and - while simplifying reality - assume that this quantitative relationship remained constant across all stratigraphic layers and time periods, with temperature as the predominant driver, the difference between glacial minima and interglacial maxima reaches ~4.9 °C (±6.3 °C). Testing whether this relationship holds under recent conditions inherits some difficulty as the species *Kalitinaia crenimargo*, consistently abundant throughout the stratigraphic record, is nowadays largely absent from the studied region, probably due to their sensitivity to anthropogenic habitat alteration. To establish a modern reference dataset, we equivalently analyzed shell isotopes of *Stenomphalia selecta*, a species with a comparable niche. While we deliberately refrain from comparing absolute values between modern shells of *Stenomphalia selecta* and subfossil shells of *Kalitinaia crenimargo* to minimize interspecific bias, the $\delta^{18}O_{precipitation}$ values calculated from $\delta^{18}O_{shell}$ (−7.93‰ at Achajur; −8.87‰ at BL) using our transfer function agree closely with the $\delta^{18}O_{precipitation}$ values extracted from modern modeled IAEA raster data (−7.5‰ and −7.64‰, respectively), corroborating the reliability of precipitation isotope reconstruction.

5.4. Synthesis of paleoclimatic evidence and future directions

Our three mollusk-based proxies - (i) ecological evidence from species composition, (ii) shell isotope signals, and (iii) assemblage-weighted climatic optima derived from niche modeling, reveal a coherent glacial-interglacial pattern in both sediment sequences. Glacial loess units L1 and L2, assigned to MIS 3, 4 and 6, record markedly cooler and drier conditions compared to units within pedocomplexes P0 and P1, that relate to interglacial stages in MIS 1 and 5. Temperature estimates based on shell-derived $\delta^{18}O_{precipitation}$ values imply an increase of ~4.9 °C in growing season temperature between the coldest glacial phases and interglacial optima. Independent evidence from pollen and leaf wax records show congruent temperature trends (Litt et al., 2014; Davis et al., 2024; Malinsky-Buller et al., 2024). However, a quantitative comparison with other empirical studies is inevitably hampered by the site-specific situation such as elevation and topography. If we compare our findings with climate model simulations for exactly the same sites, using CHELSA TraCE21k model outputs (Karger et al., 2023) which provide high-resolution (~1 km) gridded climate datasets, we get a mean annual temperature incline by about 5 °C from the LGM (~22 ka BP: 4.7 °C at Achajur; 5.3 °C at BL) to 8 ka BP (8.7 °C at Achajur; 9.45 °C at BL). This shift closely aligns with our shell-based estimates for mean growing season temperatures. However, it is important to emphasize that this comparison is qualitative in nature, as the CHELSA values refer to annual means, whereas our proxy-based reconstructions reflect growing-season conditions. CHELSA simulations further suggest that mean annual temperatures continued to incline from the Mid-Holocene to the modern (preindustrial) period by ~2 °C reaching 10.8 °C at Achajur and 11.5 °C at BL. However, empirical and model data for the Late Holocene often diverge in many regions worldwide, a discrepancy known as 'Holocene temperature conundrum' (Liu et al., 2014; Kaufman and Broadman, 2023), where proxy records generally place the Holocene thermal maximum in the mid-Holocene, while climate models tend to identify it for the present. Although our data could provide quantitative evidence for growing season temperatures, a direct comparison is complicated. Calibration based on modern shells of *Stenomphalia selecta* include a species bias, but *Kalitinaia crenimargo* is absent today at the studied sites. Shells of *Stenomphalia* show similarly high $\delta^{18}O$ values today, but species-specific offsets likely account for these differences. Owing to this and the limited temporal resolution of the younger part of the sequences, we refrain from interpreting the late Holocene interval in our dataset. Regarding annual precipitation amounts reconstructed from assemblage-weighted climatic optima, we yield a shift of up to ~270 mm between loess layers and pedocomplexes. The latter indicate annual precipitation amounts exceeding 700 mm during interglacial climatic optima within the current and last interglacial periods. By contrast, present-day means are much lower, with 481 mm at Achajur and 447 mm at BL based on WorldClim v2 gridded data (Fick and Hijmans, 2017). Consistent with these results, pollen-based and bacterial lipid biomarker (brGDGT) records from the Lake Sevan area indicate a surplus of +170 to +200 mm during mid-Holocene woodland expansion, followed by a mid-to late-Holocene decline in precipitation, temporally accompanied by prolonged drought episodes (Leroyer et al., 2016; Robles et al., 2022; Hayrapetyan et al., 2023). At the more distant Lake Van, Chevalier (2019) reconstructed pollen-based quantitative annual precipitation means of ~530 mm for the Last Glacial Maximum and ~700 mm for the last interglacial maximum, with modern precipitation amounts ranging from ~400 mm on the western to ~800 mm on the eastern shore, which is broadly consistent with our results. If we compare our data to CHELSA TraCE21k model outputs for our sites (Karger et al., 2023), annual precipitation means for the Mid-Holocene amount to 662 mm at Achajur and 658 mm at BL, but for the LGM to

greater 900 mm (917 mm at Achajur; 908 mm at BL) strongly deviating from our proxy results. CHELSA precipitation estimates for the Sevkar region would imply LGM conditions wetter than the Mid-Holocene and other interglacial maxima, whereas our proxy data indicate a drier phase instead. On the one hand, this discrepancy may reflect changing precipitation seasonality. E.g., Wolf et al. (2024) reported precipitation data from the Western Caucasus area based on speleothem $\delta^{18}O$ records and model outputs for the LGM and inferred a surplus in summer precipitation (~+50 mm) but, in parallel, a deficit in winter precipitation (of ~ -200 mm) relative to modern amounts. Higher winter precipitation totals could lead to higher annual means not equally strongly reflected in the land snail communities, as they are dormant during winter. Scenarios of comparatively moist conditions during MIS 2 are supported by lake records from the southeastern Black Sea catchment (Shumilovskikh et al., 2014) and by evidence of enhanced glacier activity in the region (Reber et al., 2014). If conditions were indeed that wet during the LGM, corresponding sediment layers would most plausibly be incorporated within the pedocomplex, and peak MIS 2 signals may therefore not be fully resolved in our sections. However, the annual precipitation amount of 900 mm suggested by the CHELSA model is not supported by the mollusk assemblages, which lack taxa indicative of closed-forest environments. Our findings are consistent with recent studies by Jarl et al. (2025), Antonosyan et al. (2024) and Rogall et al. (2025), inferring no major ecological upheavals during MIS 2. These results suggest that current climate model outputs likely overestimate absolute LGM precipitation in the Southern Caucasus area.

6. Conclusion

This study presents the first mollusk-based quantitative reconstruction of Late Quaternary climate variability in the Caucasus region. We combine three complementary approaches: (1) Gastropod assemblage analysis to infer ecological and environmental conditions, (2) Stable isotope analyses ($\delta^{18}O$ and $\delta^{13}C$) of snail shells using newly developed transfer functions, and (3) Assemblage-weighted climatic optima derived from species-climate response curves obtained through climatic niche modeling based on a dataset of 1440 modern sites from the Caucasus area. With these methods, we generate quantitative site-scale estimates of temperature and precipitation variations over the past two glacial-interglacial cycles. The results indicate mean growing season temperature of differences up to ~4.9 °C between glacial minima and interglacial maxima, and a corresponding shift in annual precipitation from ~511 mm to ~772 mm. These reconstructions provide a valuable proxy complement to existing pollen and speleothem records, helping to refine our understanding of past climate variability in this key transitional zone between Europe and Central Asia. While the dataset offers a robust empirical basis for evaluating climate model performance, further calibration studies are needed to refine niche-based reconstructions and assess potential anthropogenic biases. Our data reveal a clear discrepancy between the proxy-derived precipitation estimates and model outputs, underscoring the importance of empirical proxy evidence in climatically heterogeneous and topographically complex regions such as the Caucasus. Overall, this dataset provides a crucial benchmark for validating climate models and for contextualizing ecological thresholds relevant to vegetation dynamics and human land-use in the southern Caucasus region.

Author contributions

D. Faust and M. Fuchs acquired funding. F. Walther and B. Hausdorf conducted fieldwork and data collection. D. Wolf, H. Hovakimyan, and L. Sahakyan conducted fieldwork. M. Schneider supported the modeling work. C. Richter conducted sample processing, study design and data analysis. All authors contributed to the writing and revision of the manuscript.

Declaration of use of generative AI

The authors used ChatGPT (GPT-4; OpenAI) to improve grammar and readability of the manuscript. After using this tool, the authors reviewed and edited all content and take full responsibility for its correctness.

Declaration of competing interest

The authors declare that they have no known competing financial interests or personal relationships that could have appeared to influence the work reported in this paper.

Acknowledgement

We sincerely thank the German Research Foundation (DFG) for supporting this work in the scope of the projects number FA 239/21-1 and RI 3430/1-1. Furthermore, we acknowledge the Science Committee of the Ministry of Education, Science, Culture and Sports of the Republic of Armenia for their support within the framework of the basic state research program. We sincerely thank the two reviewers for their time and effort to review this manuscript, as well as for their valuable comments and constructive criticism, which have greatly helped to improve it.

Appendix A. Supplementary data

Supplementary data to this article can be found online at https://doi.org/10.1016/j.quascirev.2026.109937.

Data availability

All data and/or code is contained within the submission.

References

Alexandrowicz, W.P., Łanczont, M., Boguckyj, A.B., Kulesza, P., Dmytruk, R., 2014. Molluscs and ostracods of the Pleistocene loess deposits in the Halych site (Western Ukraine) and their significance for paleoenvironmental reconstructions. Quat. Sci. Rev. 105, 162–180.
Antonosyan, M., Roberts, P., Aspaturyan, N., Mkrtchyan, S., Lucas, M., Boxleitner, K., et al., 2024. Multiproxy evidence for environmental stability in the lesser caucasus during the late Pleistocene. Quat. Sci. Rev. 330, 108559.
Atkinson, T.C., Briffa, K.R., Coope, G.R., 1987. Seasonal temperatures in britain during the past 22,000 years, reconstructed using beetle remains. Nature 325, 587–592.
Banak, A., Mandic, O., Sprovieri, M., Lirer, F., Pavelić, D., 2016. Stable isotope data from loess malacofauna: evidence for climate changes in the pannonian basin during the late Pleistocene. Quat. Int. 415, 15–24.
Bray, P.J., Blockley, S.P.E., Coope, G.R., Dadswell, L.F., Elias, S.A., Lowe, J.J., Pollard, A. M., 2006. Refining mutual climatic range (MCR) quantitative estimates of paleotemperature using ubiquity analysis. Quat. Sci. Rev. 25 (15-16), 1865–1876.
Brittingham, A., Petrosyan, Z., Hepburn, J.C., Richards, M.P., Hren, M.T., Hartman, G., 2019. Influence of the north Atlantic oscillation on δD and δ18O in meteoric water in the Armenian highland. J. Hydrol. 575, 513–522.
Butler, A.J., 1972. The Food of the Terrestrial Snail Helicella virgata (Da Costa) in South Australia. PhD Thesis. University of Adelaide, p. 236.
Chevalier, M., 2019. Enabling possibilities to quantify past climate from fossil assemblages at a global scale. Global Planet. Change 175, 27–35.
Chevalier, M., 2022. Crestr: an R package to perform probabilistic climate reconstructions from palaeoecological datasets. Climate of the Past 18 (4), 821–844.
Chevalier, M., Cheddadi, R., Chase, B.M., 2014. CREST (Climate REconstruction SofTware a probability density function (PDF)-based quantitative climate reconstruction method. Clim. Past 10 (6), 2081–2098.
Chu, W., Nett, J.J., 2021. The past in dust: current trends and future directions in Pleistocene geoarcheology of European loess. J. Quat. Sci. 36 (8), 1279–1292.
Chytrý, K., Willner, W., Chytrý, M., Divíšek, J., Dullinger, S., 2022. Central European forest-steppe: an ecosystem shaped by climate, topography and disturbances. J. Biogeogr. 49 (6), 1006–1020.
Colonese, A.C., 2017. Stable isotope ecology of terrestrial gastropod shells. In: Allen, M.J. (Ed.), Molluscs in Archaeology: Methods, Approaches and Applications, vol. 3. Oxbow Books, pp. 403–405.
Dansgaard, W., 1964. Stable isotopes in precipitation. Tellus 16, 436–468.
Davis, B.A., Fasel, M., Kaplan, J.O., Russo, E., Burke, A., 2024. The climate and vegetation of Europe, northern Africa, and the Middle East during the last glacial maximum (21 000 yr BP) based on pollen data. Clim. Past 20 (9), 1939–1988.

Dettman, D.L., Sawada, Y., Pickford, M., 2024. High resolution stable isotope ratios in modern African land snails: testing inferred environmental conditions. Quat. Sci. Rev. 344, 108943.
Djamali, M., de Beaulieu, J.L., Shah-Hosseini, M., Andrieu-Ponel, V., Ponel, P., Amini, A., et al., 2008. A late Pleistocene long pollen record from Lake Urmia, NW Iran. Quat. Res. 69 (3), 413–420.
Dong, Y., Wu, N., Li, F., Zhang, D., Zhang, Y., Shen, C., Lu, H., 2022. The Holocene temperature conundrum answered by mollusk records from east Asia. Nat. Commun. 13 (1), 5153.
Dormann, C.F., Elith, J., Bacher, S., Buchmann, C., Carl, G., Carré, G., et al., 2013. Collinearity: a review of methods to deal with it and a simulation study evaluating their performance. Ecography 36 (1), 27–46.
Erdős, L., Ambarli, D., Anenkhonov, O.A., Bátori, Z., Cserhalmi, D., Kiss, M., et al., 2019. Where forests meet grasslands: forest-steppes in Eurasia. Palaearct Grasslands 40, 22–26.
Fick, S.E., Hijmans, R.J., 2017. WorldClim 2: new 1-km spatial resolution climate surfaces for global land areas. Int. J. Climatol. 37 (12), 4302–4315.
Field, R.D., 2010. Observed and modeled controls on precipitationδ18O over Europe: from local temperature to the northern annular mode. J. Geophys. Res. Atmos. 115 (D12).
Frömming, E., 1954. Biologie Der Mitteleuropäischen Landgastropoden. Berlin, Duncker & Humblot.
Gasparyan, B., Glauberman, P., 2022. Beyond European boundaries: neanderthals in the Armenian highlands and the Caucasus. In: Romagnoli, F., Rivals, F., Benazzi, S. (Eds.), Updating Neanderthals: Understanding Behavioral Complexity in the Late Middle Paleolithic. Academic Press, Elsevier, pp. 275–301.
Goodfriend, G.A., Magaritz, M., Gat, J.R., 1989. Stable isotope composition of land snail body water and its relation to environmental waters and shell carbonate. Geochem. Cosmochim. Acta 53 (12), 3215–3221.
Grimley, D.A., Counts, R.C., Conroy, J.L., Wang, H., Dendy, S.N., Nield, C.B., 2020. Last glacial maximum ecology and climate from terrestrial gastropod assemblages in Peoria loess, Western Kentucky. J. Quat. Sci. 35 (5), 650–663.
Hayrapetyan, N., Hakobyan, E., Kvavadze, E., Martinetto, E., Gabrielyan, I., Bruch, A.A., 2023. Middle to late Holocene lake level changes of Lake Sevan (Armenia)–Evidence from macro and micro plant remains of Tsovinar-1 peat section. Quat. Int. 661, 34–48.
Horsák, M., Limondin-Lozouet, N., Jurickova, L., Granai, S., Horackova, J., Legentil, C., Lozek, V., 2019. Holocene succession patterns of land snails across temperate Europe: east to west variation related to glacial refugia, climate and human impact. Paleogeogr. Paleoclimatol. Paleoecol. 524, 13–24.
Jarl, J., Gasparyan, B., Kandel, A.W., Smith, A., Bruch, A.A., 2025. A high-resolution paleoenvironmental record based on phytoliths from the Armenian highlands: the upper Paleolithic of Aghitu-3 cave. J. Archaeol. Sci.: Report 64, 105148.
Jia, Y.N., Yan, H., Dong, J., Kang, S., Wang, G., Liu, C., et al., 2024. Hydrothermal and eco-environmental evolution on the southeastern Chinese loess Plateau since the last deglaciation: evidence from terrestrial mollusk records. Quat. Sci. Rev. 331, 108648.
Karger, D.N., Lange, S., Hari, C., Reyer, C.P.O., Conrad, O., Zimmermann, N.E., Frieler, K., 2023. CHELSA-W5E5: daily 1km meteorological forcing data for climate impact studies. Earth Syst. Sci. Data 15 (6), 2445–2464. https://doi.org/10.5194/essd-15-2445-2023.
Kaufman, D.S., Broadman, E., 2023. Revisiting the Holocene global temperature conundrum. Nature 614 (7948), 425–435.
Lécolle, P., 1985. The oxygen isotope composition of land snail shells as a climatic indicator: applications to hydrogeology and paleoclimatology. Chem. Geol.: Isot. Geosci. Seq. 58 (1), 157–181.
Lehmkuhl, F., Schulte, P., Römer, W., Pötter, S., 2023. The loess landscapes of the lower rhine embayment as (geo-) archeological archives–insights and challenges from a geomorphological and sedimentological perspective. E&G Quat. Sci. J. 72 (2), 203–218.
Leroyer, C., Joannin, S., Aoustin, D., Ali, A.A., Peyron, O., Ollivier, V., et al., 2016. Mid Holocene vegetation reconstruction from vanevan peat (south-eastern shore of Lake Sevan, Armenia). Quat. Int. 395, 5–18.
Lipińska, A.M., Książkiewicz, Z., Ćmiel, A.M., Hnatyna, O., Laskowska, P., Halabowski, D., 2025. Winter activity and dormancy of snails: Freezing and food shortage avoidance strategy facing snow-cover shortage. Animals: Open Access J. MDPI 15 (3), 348.
Litt, T., Pickarski, N., Heumann, G., Stockhecke, M., Tzedakis, P.C., 2014. A 600,000 year long continental pollen record from Lake Van, eastern Anatolia (Turkey). Quat. Sci. Rev. 104, 30–41.
Liu, Z., Gu, Z., Wu, N., Xu, B., 2007. Diet control on carbon isotopic composition of land snail shell carbonate. Chin. Sci. Bull. 52 (3), 388–394.
Liu, Z., Zhu, J., Rosenthal, Y., Zhang, X., Otto-Bliesner, B.L., Timmermann, A., et al., 2014. The Holocene temperature conundrum. Proc. Natl. Acad. Sci. 111 (34), E3501–E3505.
Lomax, J., Wolf, D., Wolpert, U.T., Sahakyan, L., Hovakimyan, H., Faust, D., Fuchs, M., 2021. Establishing a luminescence-based chronostratigraphy for the last glacial-interglacial cycle of the loess-paleosol sequence achajur (Armenia). Front. Earth Sci. 9, 755084.
Ložek, V., 1990. Molluscs in loess, their paleoecological significance and role in geochronology - principles and methods. Quat. lnternat. 7 (8), 71–79.
Lydolph, P.E., 1977. Climates of the Soviet Union. Elsevier Scientific Publishing Company, Amsterdam.
Malinsky-Buller, A., Edeltin, L., Ollivier, V., Joannin, S., Peyron, O., Lauer, T., et al., 2024. The environmental and cultural background for the reoccupation of the Armenian highlands after the last glacial maximum: the contribution of kalavan 6. J. Archaeol. Sci.: Report 56, 104540.
Mellars, P., 2004. Neanderthals and the modern human colonization of Europe. Nature 432 (7016), 461–465.
Metref, S., Rousseau, D.D., Bentaleb, I., Labonne, M., Vianey-Liaud, M., 2003. Study of the diet effect on δ13C of shell carbonate of the land snail helix aspersa in experimental conditions. Earth Planet Sci. Lett. 211 (3), 381–393.
Moine, O., Rousseau, D.D., Jolly, D., Vianey-Liaud, M., 2002. Paleoclimatic reconstruction using mutual climatic range on terrestrial mollusks. Quat. Res. 57 (1), 162–172.
Muscarella, R., Galante, P.J., Soley-Guardia, M., Boria, R.A., Kass, J.M., Uriarte, M., Anderson, R.P., 2014. ENM eval: an R package for conducting spatially independent evaluations and estimating optimal model complexity for maxent ecological niche models. Methods Ecol. Evol. 5 (11), 1198–1205.
Myers, N., Mittermeier, R.A., Mittermeier, C.G., Da Fonseca, G.A., Kent, J., 2000. Biodiversity hotspots for conservation priorities. Nature 403 (6772), 853–858.
Nield, C.B., Yanes, Y., Pigati, J.S., Rech, J.A., von Proschwitz, T., Nekola, J.C., 2022. Oxygen isotopes of land snail shells in high latitude regions. Quat. Sci. Rev. 279, 107382.
Obreht, I., Hambach, U., Veres, D., Zeeden, C., Bösken, J., Stevens, T., et al., 2017. Shift of large-scale atmospheric systems over Europe during late MIS 3 and implications for modern human dispersal. Sci. Rep. 7 (1), 5848.
Phillips, S.J., Anderson, R.P., Schapire, R.E., 2006. Maximum entropy modeling of species geographic distributions. Ecol. Model. 190 (3-4), 231–259.
Phillips, S.J., Anderson, R.P., Dudík, M., Schapire, R.E., Blair, M.E., 2017. Opening the black box: an open-source release of maxent. Ecography 40 (7), 887–893.
Pickarski, N., Litt, T., 2017. A new high-resolution pollen sequence at Lake Van, Turkey: insights into penultimate interglacial–glacial climate change on vegetation history. Clim. Past 13 (6), 689–710.
Reber, R., et al., 2014. Glacier advances in northeastern Turkey before and during the global last glacial maximum. Quat. Sci. Rev. 101, 177–192.
Richter, C., Wolf, D., Walther, F., Meng, S., Sahakyan, L., Hovakimyan, H., Wolpert, T., Fuchs, M., Faust, D., 2020. New insights into southern Caucasian glacial–interglacial climate conditions inferred from Quaternary gastropod fauna. J. Quat. Sci. 35 (5), 634–649.
Richter, C., Roettig, C.B., Wolf, D., Gärtner, A., Kolb, T., Faust, D., 2021. Climate shifts vs. edaphic humidity and the difficulty of paleoreconstructions - a malacological study on stable isotopes in Quaternary dune sequences of fuerteventura. J. Quat. Sci. 36 (3), 426–440.
Richter, C., Walther, F., Meng, S., Reip, H., Schneider, M., Joachimski, M.M., Horsák, M., 2025. Land snail shell δ18O records in periglacial loess deposits: new transfer functions for precipitation δ18O and temperature in dry continental settings. Quat. Sci. Rev. 363, 109440.
Robles, M., Peyron, O., Brugiapaglia, E., Ménot, G., Dugerdil, L., Ollivier, V., et al., 2022. Impact of climate changes on vegetation and human societies during the Holocene in the south caucasus (Vanevan, Armenia). A multiproxy approach including pollen, NPPs and brGDGTs. Quat. Sci. Rev. 277, 107297.
Rogall, D.L., Blain, Hugues-Alexandre, Oikonomou, Ioannis A.K., Karampaglidis, Theodoros, Petrosyan, Artur, Gasparyan, Boris, Malinsky-Buller, Ariel, 2025. Comparing past and present. The Holocene and marine isotope stage 3 microvertebrate assemblage of Ararat-1 cave. Quat. Sci. Rev. 366, 109512.
Rousseau, D.D., 1991. Climatic transfer function from Quaternary molluscs in European loess deposits. Quat. Res. 36 (2), 195–209.
Rousseau, D.D., Bagniewski, W., Sun, Y., 2023. Detection of abrupt changes in East Asian monsoon from Chinese loess and speleothem records. Global Planet. Change 227, 104154.
Rozanski, K., Araguás-Araguás, L., Gonfiantini, R., 1993. Isotopic patterns in modern global precipitation. In: Union, A.G. (Ed.), Climate Change in Continental Isotopic Records, vol. 78. American Geophysical Union Geophysical Monograph, American Washington DC, pp. 1–36.
Schmid, G., 1930. Zur Biologie der Helicella obvia Hartm. Arch. Molluskenkd. 62, 57–71.
Schmid, G., 1934. Zur Biologie von Helicella ericetorum (Müll.). Arch. Molluskenkd. 33, 201–207.
Schmitt, K.E., Beuzen-Waller, T., Schmidt, C., Proctor, L., Lindauer, S., Gey, C.J., et al., 2024. Melanoides tuberculata and Zootecus insularis gastropod shells provide a snapshot into past hydroclimatic conditions of arid environments: new perspectives from Oman. Palaeogeogr. Palaeoclimatol. Palaeoecol. 655, 112542.
Schmitt, K.E., Proctor, L., Beuzen-Waller, T., Schmidt, C., Lindauer, S., Jean, M., et al., 2025. Unlocking the potential of the terrestrial gastropod species Zootecus insularis as a climate archive for arid regions. Sci. Rep. 15 (1), 13754.
Shumilovskikh, L.S., Fleitmann, D., Nowaczyk, N.R., Behling, H., Marret, F., Wegwerth, A., Arz, H.W., 2014. Orbital-and millennial-scale environmental changes between 64 and 20 ka BP recorded in black sea sediments. Clim. Past 10 (3), 939–954.
Sümegi, P., 2019. Refuting ideas based on a small batch of data: malacothermometry aid in the reconstruction of mean July paleo-temperatures in the carpathian basin for the last glacial of the Pleistocene. Archeometriai Műhely XVI/3 143–166.
Sun, Y., Clemens, S.C., Guo, F., Liu, X., Wang, Y., Yan, Y., Liang, L., 2021. High-sedimentation-rate loess records: a new window into understanding orbital-and millennial-scale monsoon variability. Earth Sci. Rev. 220, 103731.
Terzer-Wassmuth, S., Wassenaar, L.I., Welker, J.M., Araguás-Araguás, L.J., 2021. Improved high-resolution global and regionalized isoscapes of δ 18O, δ 2H and d-excess in precipitation. Hydrol. Process. 35 (6), e14254.
Újvári, G., Bernasconi, S.M., Stevens, T., Kele, S., Páll-Gergely, B., Surányi, G., Demény, A., 2021. Stadial-interstadial temperature and aridity variations in east central Europe preceding the last glacial maximum. Paleoceanogr. Paleoclimatol. 36 (8) e2020PA004170.

Wang, M., Wang, Xin, Dettman, David L., Wang, Qiang, Wu, Donghao, Liu, Weiguo, Khomali, Farhad, Nie, Junsheng, Wu, Naiqin, Chen, Fahu, 2024. Stable carbon isotope composition of land snail shells in westerlies Asia and monsoonal Asia: paleoclimate implications. Quat. Sci. Rev. 327, 108505.

Wei, F., Dong, Y., Wu, N., Li, F., Lu, H., 2025. Assessing the temporal stability of snail-climate relationships since the last glacial maximum: insights from boosted regression trees and LOESS models. Palaeogeogr. Palaeoclimatol. Palaeoecol. 662, 112771.

Wolf, D., Baumgart, P., Meszner, S., Fülling, A., Haubold, F., Sahakyan, L., Meliksetian, K., Faust, D., 2016. Loess in Armenia- stratigraphic findings and paleoenvironmental indications. PGA (Proc. Geol. Assoc.) 127 (1), 29–39.

Wolf, D., Lomax, J., Sahakyan, L., Hovakimyan, H., Profe, J., Schulte, P., et al., 2022. Last glacial loess dynamics in the southern caucasus (NE-Armenia) and the phenomenon of missing loess deposition during MIS-2. Sci. Rep. 12 (1), 13269.

Wolf, A., Baker, J.L., Tjallingii, R., Cai, Y., Osinzev, A., Antonosyan, M., et al., 2024. Western caucasus regional hydroclimate controlled by cold-season temperature variability since the last glacial maximum. Commun. Earth Environ. 5 (1), 66.

Yanes, Y., Delgado, A., Castillo, C., Alonso, M.R., Ibáñez, M., De la Nuez, J., Kowalewski, M., 2008. Stable isotope (δ18O, δ13C, and δD) signatures of recent terrestrial communities from a low-latitude, oceanic setting: endemic land snails, plants, rain, and carbonate sediments from the eastern Canary Islands. Chem. Geol. 249 (3-4), 377–392.

Yanes, Y., Asta, M.P., Ibáñez, M., Alonso, M.R., Romanek, C.S., 2013. Paleoenvironmental implications of carbon stable isotope composition of land snail tissues. Quat. Res. 80 (3), 596–605.

Zanchetta, G., Leone, G., Fallick, A.E., Bonadonna, F.P., 2005. Oxygen isotope composition of living land snail shells: data from Italy. Paleogeogr. Paleoclimatol. Paleoecol. 223 (1), 20–33.

Zazanashvili, N., Sanadiradze, G., Bukhnikashvili, A., Kandaurov, A., Tarkhnishvili, D., 2004. Caucasus. In: Mittermaier, R.A., Gil, P.G., Hoffmann, M., Pilgrim, J., Brooks, T., Mittermaier, C.G., Lamoreux, J., Da Fonseca, G.A.B. (Eds.), Hotspots Revisited. Earth's Biologically Richest and Most Endangered Terrestrial Ecoregions. CEMEX/Agrupacion Sierra Madre, Sierra Madre, pp. 148–153.

Zomer, R.J., Xu, J., Trabucco, A., 2022. Version 3 of the global aridity index and potential evapotranspiration database. Sci. Data 9 (1), 409.